Two- and three-pion quantum statistics correlations in Pb-Pb collisions at $\sqrt{s_{NN}} = 2.76$ TeV at the CERN Large Hadron Collider

B. Abelev *et al.*[*]
(ALICE Collaboration)

(Received 1 November 2013; revised manuscript received 29 January 2014; published 26 February 2014)

Correlations induced by quantum statistics are sensitive to the spatiotemporal extent as well as dynamics of particle-emitting sources in heavy-ion collisions. In addition, such correlations can be used to search for the presence of a coherent component of pion production. Two- and three-pion correlations of same and mixed charge are measured at low relative momentum to estimate the coherent fraction of charged pions in Pb-Pb collisions at $\sqrt{s_{NN}} = 2.76$ TeV at the CERN Large Hadron Collider with ALICE. The genuine three-pion quantum statistics correlation is found to be suppressed relative to the two-pion correlation based on the assumption of fully chaotic pion emission. The suppression is observed to decrease with triplet momentum. The observed suppression at low triplet momentum may correspond to a coherent fraction in charged-pion emission of $23\% \pm 8\%$.

DOI: 10.1103/PhysRevC.89.024911 PACS number(s): 25.75.Gz, 05.30.Jp

I. INTRODUCTION

The techniques of intensity interferometry are often used to extract information of the space-time structure of particle-emitting sources [1]. For identical boson correlations, quantum statistics (QS) or Bose-Einstein correlations contribute significantly at low relative momentum. The strength of QS correlations is known to depend on the degree of chaoticity of particle-emitting sources [2,3]. Identical boson QS correlations reach their maximum value for fully chaotic sources (no coherence) and their minimum value for fully coherent sources. The possibility of coherent pion production in high-energy heavy-ion collisions has been considered several times before. In particular, it was proposed that the interior of the high-energy hadron collisions might form a Bose-Einstein condensate [4] with an anomalous chiral order parameter (DCC) [5]. Such a condensate produced in the interior may survive until some time after the relatively hot and chaotic expanding shell decouples and hadronizes. The pion radiation from a condensate is expected to be coherent and thus suppresses Bose-Einstein correlations. Furthermore, initial conditions such as the color-glass condensate (CGC) [6], which invoke the coherent production of partons, might also lead to condensate formation [7]. In this article we present two- and three-pion correlations of same and mixed charge at low relative momentum to estimate the coherent fraction of charged-pion emission in Pb-Pb collisions at $\sqrt{s_{NN}} = 2.76$ TeV at the LHC with ALICE.

A number of past experimental efforts have been made to measure the degree of coherence in high-energy heavy-ion collisions using three-pion Bose-Einstein correlations: NA44, WA98, and STAR [8–10]. The methodology used here represents an improvement over the past efforts, which we summarize in Sec. III.

The remainder of this article is organized into six sections. In Sec. II we describe the data-selection procedure. In Sec. III we introduce the methodology used in this analysis. In Sec. IV we describe the treatment of final-state interactions (FSIs). In Sec. V we describe the treatment of momentum resolution corrections. In Sec. VII we explain the estimation of systematic uncertainties. In Sec. VIII we present the results of this analysis. We conclude with a possible interpretation of the analysis results in Sec. IX.

II. EXPERIMENT AND DATA ANALYSIS

Data were taken from the 2011 Pb-Pb run at $\sqrt{s_{NN}} = 2.76$ TeV at the CERN Large Hadron Collider (LHC) with ALICE [11]. The VZERO detectors [12], located in the forward and backward regions of the detector, were used to form a minimum-bias trigger by requiring a simultaneous signal in both [13]. The charged-particle multiplicity in the VZERO detectors is used to determine the collision centrality. Approximately 34×10^6 minimum-bias collisions were used in this analysis. Particle tracking was performed with two azimuthally complete detectors: the inner tracking system (ITS) and the time projection chamber (TPC) [14]. The ITS consists of six layers of silicon detectors: silicon pixel (layers 1–2), silicon strip (layers 3–4), and silicon drift (layers 5–6) detectors. The combined number of readout channels for all six layers is 1.257×10^7. The ITS provides high spatial resolution to the distance of closest approach (DCA) of a particle to the primary vertex. However, it was not used for the momentum determination of particles in this analysis. Cluster sharing within the ITS was found to cause a slight increase in track merging, to which this analysis is especially sensitive. The TPC was used to determine the particle's momenta and charge via its radius of curvature in the 0.5-T longitudinal magnetic field. The TPC is composed of 159 radially aligned pad rows for each of the 18 azimuthal sectors, totaling 557 568 readout channels.

In addition to the tracking capabilities, the ITS and TPC provide particle identification capabilities through the specific ionization energy loss (dE/dx) in the silicon layers and

[*]Full author list given at the end of the article.

TPC gas, respectively. We select charged pions within 2 standard deviations (σ) of the expected pion dE/dx value. For momenta greater than 0.6 GeV/c, high pion purity is maintained with the time-of-flight (TOF) detector. The TOF covers the full azimuthal range and the pseudorapidity range $|\eta| < 0.9$, except for the region $260^\circ < \varphi < 320^\circ$, where no TOF modules were installed to reduce the material budget in front of the photon spectrometer. With TOF we select tracks within 2σ of the expected pion TOF values. Tracks which are within 2σ of the expected kaon or proton dE/dx or TOF values are rejected. Below 0.45 GeV/c we further reject pion candidates if their dE/dx is within 2σ of the expected electron dE/dx value. The pion-pair purity in this analysis is estimated to range from 90% to 94% for the highest and lowest pair momentum, respectively.

To ensure uniform tracking in the ITS, TPC, and TOF we require the z coordinate of the primary vertex to be within a distance of 10 cm from the detector center. We analyze tracks with transverse momenta in the interval $0.16 < p_{\mathrm{T}} < 1.0$ GeV/c and pseudorapidity $|\eta| < 0.8$. To ensure good momentum resolution, we require a minimum of 70 tracking points in the TPC.

Track merging and splitting are known issues for same-charge tracks at very low relative momentum [15]. We minimize the contribution from merged and split pairs through three types of pair cuts. First, we simply reject all pairs whose Lorentz invariant relative momentum, q, is less than 5 MeV/c. Second, we reject all pairs whose angular separation is less than 0.02 and 0.045 rad in the longitudinal and azimuthal direction, respectively. The pair angular separation is evaluated at a radial distance of 1.0 and 1.6 m, where the most pronounced track-merging and -splitting effects were observed, respectively. Third, we reject pairs that share more than 5% of pad-row tracking points [16]. These three cuts are applied to all terms of the correlation functions (same-event and mixed-event) introduced in the next section. For three-pion correlations we apply these three cuts to each of the three pairs in the triplet. The cuts are only applied to same-charge pairs. Mixed-charge pairs are easily distinguished in the central barrel magnetic field as their trajectories are bent away from each other.

III. METHODOLOGY

Two-particle correlation functions are binned in narrow intervals of the mean pair transverse momentum, $k_{\mathrm{T}} = |\mathbf{p}_{\mathrm{T},1} + \mathbf{p}_{\mathrm{T},2}|/2$, and Lorentz invariant relative momenta, $q = \sqrt{-(p_1 - p_2)^\mu (p_1 - p_2)_\mu}$. They are defined as the ratio of the inclusive two-particle spectrum, $N_2(p_1, p_2)$ over the product of inclusive single-particle spectra, $N_1(p_1)N_1(p_2)$:

$$C_2(p_1, p_2) = \frac{N_2(p_1, p_2)}{N_1(p_1)N_1(p_2)}. \tag{1}$$

The numerator of the correlation function is formed by all pairs of particles from the same event. The denominator is formed by taking one particle from one event and the second particle from another event. The same- and mixed-event two-particle distributions are normalized to each other in the interval $0.15 < q < 0.175$ GeV/c, sufficiently above the dominant region of low relative momentum correlations and sufficiently narrow to avoid the small influence of background correlations. Only events within the same centrality class are mixed. The centrality classes correspond to the top 0%–5% through 45%–50% of the particle multiplicity distribution estimated with the VZERO detector. Each class has a width of 5%.

The isolation of genuine two-pion correlations is complicated by several additional factors. Namely, the resolvable threshold of low relative momentum pairs is limited by track merging and splitting in the ALICE detector. The QS correlation of long-lived resonance decays is largely localized below this threshold and is therefore unobservable. This leads to an apparent decrease of QS correlations and is described by the λ or "dilution" parameter in this analysis. Given λ, two-particle correlations can be written as

$$N_2(p_1, p_2) = \mathcal{N}\big[(1-\lambda)N_1(p_1)N_1(p_2) + \lambda K_2(q) N_2^{\mathrm{QS}}(p_1, p_2)\big], \tag{2}$$

$$C_2(q) = \mathcal{N}\big[(1-\lambda) + \lambda K_2(q) C_2^{\mathrm{QS}}(q)\big], \tag{3}$$

where $\mathcal{N}$ is a residual normalization taking into account the small nonfemtoscopic contributions [17,18]. We allow a different $\mathcal{N}$ for same and mixed-charge correlations as the nonfemtoscopic contributions can be different. $K_2(q)$ is the FSI correlation. N_2^{QS} and $C_2^{\mathrm{QS}}(q)$ are the genuine two-pion QS distribution and correlation, respectively. Here, unlike in most experimental publications on this subject, the λ parameter does not include effects of partial coherence. Its deviation below unity can also be attributable to secondary contamination, pion misidentification, and finite q binning. Same-charge pion QS correlations excluding coherence can be parametrized by

$$C_2^{\mathrm{QS},++}(q) = 1 + E_{\mathrm{w}}(R_{\mathrm{ch}}q)^2 e^{-R_{\mathrm{ch}}^2 q^2}, \tag{4}$$

$$E_{\mathrm{w}}(R_{\mathrm{ch}}q) = 1 + \sum_{n=3}^{\infty} \frac{\kappa_n}{n!(\sqrt{2})^n} H_n(R_{\mathrm{ch}}q), \tag{5}$$

where R_{ch} are the characteristic radii of the chaotic component. $E_{\mathrm{w}}(R_{\mathrm{ch}}q)$ is the Edgeworth expansion characterizing deviations from Gaussian behavior [19]. H_n are the Hermite polynomials and κ_n are the Edgeworth coefficients. The first two relevant Edgeworth coefficients (κ_3,κ_4) are found to be sufficient to describe the non-Gaussian features in this analysis. At the two-pion level we do not include an explicit parametrization of a possible coherent component owing to the large uncertainty of non-Gaussian Bose-Einstein correlations. In this analysis we assume λ of mixed-charge pions is identical to that of same-charge pions: $\lambda^{+-} = \lambda^{\pm\pm}$. This is a valid assumption at high energies where the secondary contamination from particles and antiparticles are expected to be equal [20].

Three-particle correlation functions are binned in terms of the three invariant relative momenta in the triplet: q_{12}, q_{31}, and q_{23}. The three-particle correlation function is similarly the ratio of the inclusive three-particle spectrum to the product of the inclusive single-particle spectra binned in the pair relative momenta:

$$C_3(p_1, p_2, p_3) = \frac{N_3(p_1, p_2, p_3)}{N_1(p_1)N_1(p_2)N_1(p_3)}, \tag{6}$$

$$Q_3 = \sqrt{q_{12}^2 + q_{31}^2 + q_{23}^2}. \tag{7}$$

The numerator of C_3 is formed by all triplets of particles from the same event. The denominator is formed by taking each of the three particles from different events. We project three-particle correlations against the Lorentz invariant Q_3.

For three-particle correlations, $\lambda \neq 1$ similarly causes "feed-up" from pure combinatorial distributions and two-particle correlations as described in Eq. (8) below. The derivation of Eq. (8) is shown in the Appendix. In Eq. (8), $N_2(p_i,p_j)N_1(p_k)$ terms represent the case where particles i and j are taken from the same event, while particle k is taken from a different event and K_3 is the three-pion FSI correlation. Isolation of the three-pion QS correlation is done by solving Eq. (8) for $N_3^{\rm QS}$. Using $N_2^{\rm QS}$ and $N_3^{\rm QS}$ one can construct a cumulant correlation function, $\mathbf{c}_3$, in Eq. (9):

$$N_3(p_1,p_2,p_3) = f_1N_1(p_1)N_1(p_2)N_1(p_3) + f_2[N_2(p_1,p_2)N_1(p_3) + N_2(p_3,p_1)N_1(p_2) + N_2(p_2,p_3)N_1(p_1)] + f_3K_3(q_{12},q_{31},q_{23})N_3^{\rm QS}(p_1,p_2,p_3), \tag{8}$$

$$\mathbf{c}_3(p_1,p_2,p_3) = 1 + \big[2N_1(p_1)N_1(p_2)N_1(p_3) - N_2^{\rm QS}(p_1,p_2)N_1(p_3) - N_2^{\rm QS}(p_3,p_1)N_1(p_2) - N_2^{\rm QS}(p_2,p_3)N_1(p_1) + N_3^{\rm QS}(p_1,p_2,p_3)\big]\big/N_1(p_1)N_1(p_2)N_1(p_3). \tag{9}$$

In Eq. (8), f_1, f_2, and f_3 are derived in the Appendix and are given by $(1-\lambda^{1/2})^3 + 3\lambda^{1/2}(1-\lambda^{1/2})^2 - 3(1-\lambda^{1/2})(1-\lambda)$, $(1-\lambda^{1/2})$, $\lambda^{3/2}$, respectively.

The quantity in square brackets in Eq. (9) represents a three-pion cumulant which has all two-pion correlations removed. Therefore, the three-pion cumulant represents the isolation of genuine three-pion QS correlations. All same- and mixed-event three-particle distributions are normalized to each other in the range where all three pairs satisfy $0.15 < q_{ij} < 0.175$ GeV/c, sufficiently above the dominant region of low relative momentum correlations and sufficiently narrow to avoid the small influence of background correlations.

The novel effects measured with three-particle correlations are isolated with the r_3 function [21,22]:

$$r_3(p_1,p_2,p_3) = \frac{\mathbf{c}_3(p_1,p_2,p_3) - 1}{\sqrt{\big[C_2^{\rm QS}(p_1,p_2) - 1\big]\big[C_2^{\rm QS}(p_3,p_1) - 1\big]\big[C_2^{\rm QS}(p_2,p_3) - 1\big]}}. \tag{10}$$

The r_3 function isolates the phase of three-pion correlations: $r_3 = I\cos(\Phi) \approx I(1-\Phi^2/2)$ [21]. The intercept of r_3, I, is expected to be 2 in the case of fully chaotic particle-emitting sources and less than 2 in the case of partially coherent sources. The leading-order contribution to the phase was shown to be quadratic in relative momenta, $\Phi \approx a_{\mu\nu}q_{12}^{\mu}q_{23}^{\nu}$, which leads to quartic behavior in r_3 [21]. The antisymmetric tensor $a_{\mu\nu}$ characterizes space and momentum source asymmetries related to how the spatial position of maximum pion emission changes with momentum. There are six nonvanishing independent components in $a_{\mu\nu}$. However, owing to limited statistical precision we project r_3 from three-dimensional invariant relative momenta to one-dimensional Q_3. A fit quartic and quadratic in Q_3 is performed,

$$r_3(Q_3) = I\big(1 - aQ_3^4\big), \tag{11}$$

$$r_3(Q_3) = I\big(1 - aQ_3^2\big), \tag{12}$$

where I is the intercept of r_3 [$I = r_3(0)$], and a is the quartic or quadratic coefficient. The quadratic fit is motivated by previous fit attempts by the STAR collaboration [10]. The coherent fraction (G) can be extracted from the intercept as [21]

$$I = 2\sqrt{1-G}\,\frac{1+2G}{(1+G)^{3/2}}. \tag{13}$$

Equation (13) neglects the effect of the charge constraint on charged coherent states [20,23,24]. In the quantum optics approach to coherent states [25], charged pions can only be in coherent states when positive and negative pions pair together to form a charge neutral state. However, because the charge constraint affects both numerator and denominator of r_3 in the same direction, its effect on r_3 for $G < 30\%$ is expected to increase its intercept by less than 17% [24].

The denominator of r_3 is measured using the three-particle combinatorial distribution and two-particle correlation strengths. The two-particle correlation strengths are tabulated from a previous run over the data. They are tabulated in sufficiently narrow intervals or bins of centrality, $k_{\rm T}$, and three-dimensional (3D) relative momentum to allow reliable interpolation between bins. We bin the two-particle correlations in nine centrality bins (5% wide) and 4 $k_{\rm T}$ bins in the longitudinally comoving system (LCMS). Forty $q_{\rm out}$, $q_{\rm side}$, and $q_{\rm long}$ bins (5 MeV/c wide) are chosen. $q_{\rm out}$ is the projection of the relative momentum along the pair momentum direction. $q_{\rm long}$ is the projection along the beamline. $q_{\rm side}$ is then perpendicular to the other two (azimuthal projection). The four $k_{\rm T}$ bins are chosen such that they divide the pair distribution into four equally populated intervals.

A. Methodology improvement

The methodology used here to measure three-pion QS correlations represents an improvement over the past efforts [8–10], which we highlight here.

(i) In addition to QS correlations, charged pions also experience a Coulomb repulsion, which reduces the apparent strength of QS correlations. Corrections for the three-body Coulomb interactions are damped in this analysis according to the observed λ parameter.

Previously, the Coulomb corrections were undamped and thus overestimated.

(ii) The Coulomb corrections are estimated by integrating over an assumed freeze-out distribution of pions. We take into account the effect of resonance decays on the freeze-out distribution. Previously, a Gaussian distribution was assumed.

(iii) For the case when $\lambda < 1$, the measured three-pion correlations contain a feed-up from lower-order correlations, which is now removed.

(iv) We apply momentum resolution corrections, which was not universally done in the past efforts.

(v) We apply corrections for muon contamination which was not done in the past efforts.

(vi) The isolation of the cumulants is done at the pair/triplet distribution level instead of at the correlation function level.

(vii) Mixed-charge two- and three-pion correlations are used to help determine the λ parameter and to monitor the performance of FSI corrections.

IV. FINAL-STATE INTERACTIONS

The treatment of FSIs is crucial for this analysis. In addition to QS correlations, identical charged pions also experience FSIs which reduce the apparent strength of QS correlations. The FSIs of charged pions are dominated by the Coulomb interaction. The strong interactions, while small for same-charge pions, are important for mixed-charge pions. Coulomb and strong FSI corrections are included in this analysis for both two- and three-particle same- and mixed-charge correlations. The wave functions for two-pion Coulomb and strong FSIs are known to high precision [26]. Two-pion FSIs are calculated by averaging the modulus square of the two-pion FSI wave functions over an assumed freeze-out particle-emitting source distribution. This is then divided by the corresponding average of plane-wave functions to isolate the pure FSIs. For same-charge pions, the wave functions are symmetrized. Typically, the source distribution is taken to be a spherical Gaussian with a radius matching what is found in the data. Here, we use a more sophisticated approach. All FSIs are calculated directly within THERMINATOR 2 events [27,28]. The pair relative separation at freeze-out in the pair-rest frame, r^*, as well as the space-momentum correlations included in the model are used. THERMINATOR includes all of the known resonance decays. Pions from resonance decays add non-Gaussian features to the freeze-out distribution. Furthermore, they increase the mean value of r^*, which in turn reduces the strength of FSI correlations. The same centrality class and k_{T} range from the data are used to calculate the FSIs. The freeze-out hypersurfaces in THERMINATOR were calculated within 3D viscous hydrodynamics with an initial and final temperature of 512 and 140 MeV, respectively. The starting time for hydrodynamics was 0.6 fm/c.

Three-body FSI wave functions are not known for all regions of phase-space. However, all asymptotic wave functions are known [29]. In particular, the wave-function corresponding to the phase-space region where all three interparticle spacings are large, Ω_0, is given by the product of the three two-body wave functions. It has been shown that the Ω_0 wave function is a justified approximation also in the case where the triplet kinetic energy in the triplet rest frame is sufficiently large [30]. It is estimated that triplet energies exceeding $\sim$7 MeV for 6-fm sources justify the use of the Ω_0 wave function. The minimum triplet energy considered in this analysis is $\sqrt{3} \times 5 \approx 8.7$ MeV when all three pair q's are at their minimum allowed value of 5 MeV/c.

For the case of same-charge pion FSIs with the Ω_0 wave function, the modulus square of the fully symmetrized FSI wave-function is averaged in THERMINATOR events. This is then divided by the corresponding average of fully symmetrized plane waves. The full symmetrization assumes fully chaotic emission. For the case of mixed-charge FSIs, only the same-charge pairs are symmetrized. All K factors in this analysis are averaged over the THERMINATOR freeze-out distribution for pairs satisfying $r^* < 80$ fm. For the K_3 calculation, all three pairs must satisfy this requirement.

All three-pion correlations in this analysis are binned in 3D corresponding to the three pair invariant relative momenta: q_{12}, q_{23}, q_{31}. The three-pion FSI correlations are likewise calculated in 3D for the integrated k_{T} range.

Another more commonly used approach to treat three-body FSIs is the Riverside approach [31] for which the three-body FSI correlation, K_3, is given by the triple product of Gamov factors ($K_3 = G^{12}G^{23}G^{31}$). In the generalized version of this approach, "generalized Riverside" (GRS), each two-body factor is averaged over the assumed source distribution ($K_3 = K_2^{12}K_2^{23}K_2^{31}$) [9,10]. In Fig. 1 we compare our calculations of three-body FSI correlations using the Ω_0 wave function and GRS approach within THERMINATOR events. We observe similar FSI correlations with both methods.

V. MOMENTUM RESOLUTION

Finite momentum resolution in the ALICE detector generally causes a smearing of the correlation function. We estimate its effect on the correlation functions by assigning a weight to each pair or triplet in HIJING [32] based on the measured correlation strength in real data. The same weight is applied to two versions of each N_n ($n = 1,2,3$) histogram. The first is filled with the nonsmeared ideal q from HIJING. The second is filled with the smeared q after the tracks have been propagated through the simulation of the ALICE detector response. The ratio of the first to the second histogram forms the correction factor for the N_n distributions.

The momentum resolution corrections are found to be largest at low $q(Q_3)$, where they increase the raw correlation function by less than 5% (8%) for two-pion (three-pion) correlations. We also observe that the correction factors do not change significantly with k_{T}. After the momentum resolution corrections are applied, we verified that the observed correlation strength and shape matches the assumed values used as a weight in HIJING.

VI. MUON CONTAMINATION

The pion-pair purity is estimated to be about 93% in HIJING with the simulated ALICE detector response. The

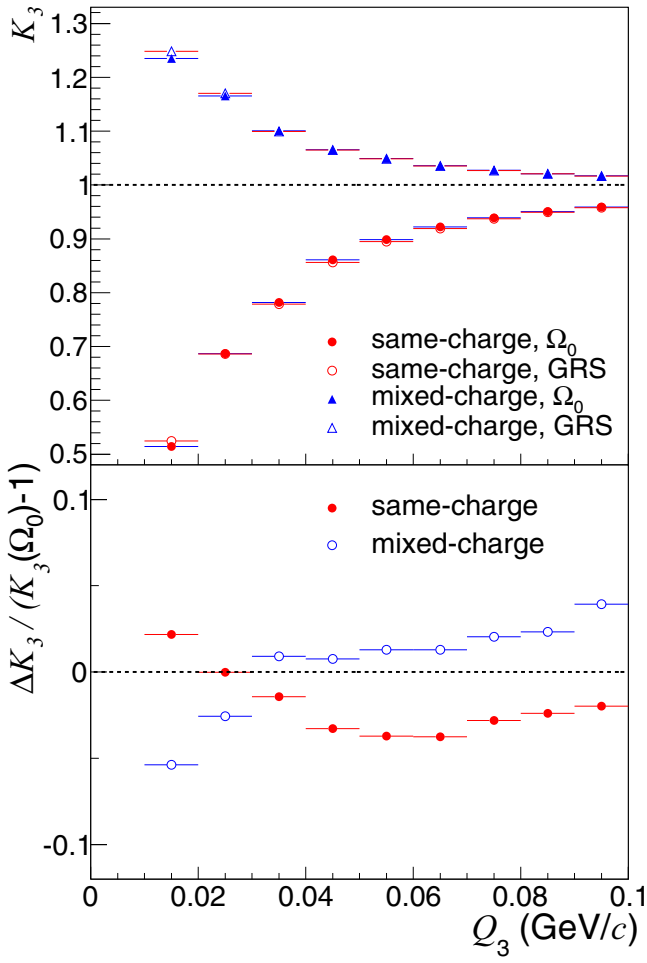

FIG. 1. (Color online) Comparison of same- and mixed-charge three-pion FSI correlations. Ω_0 wave function and generalized Riverside (GRS) method are shown. The calculation was performed in THERMINATOR (0%–5%). The bottom panel shows the difference between the two methods, $\Delta K_3 = K_3(\Omega_0) - K_3(\mathrm{GRS})$, divided by $K_3(\Omega_0) - 1$.

leading order misidentified pair is the muon pion combination. The rest of the misidentified combinations taken together contribute less than 1% to the total pairs. We estimate that about 93% of the muons contaminating our sample originate from primary-pion decays. The primary parent pion is expected to interact with the other primary pions via QS + FSI. We therefore expect that the muon pion pairs contaminating our sample will contain a residual pion pion correlation. For the three-pion case the muon pion pion combination dominants the misidentified triplets. We form a correction factor for all two-pion (three-pion) terms by assigning a QS + FSI weight to the parent pions in the pair (triplet) which subsequently decayed into muons. A smeared correlation is obtained when the assigned correlation is binned in relative momentum using the muon momentum. The ratio of the assigned correlation to the smeared correlation forms our correction factor. The correction is applied to same and mixed-charge correlations and is found to increase λ by about 5% while having a negligible effect on the extracted radii. The correction increases the two-pion correlation by about 1.5% at low q and rapidly decreases for larger q. The correction increases the three-pion correlation by about 3% at low Q_3 and by about 1% for high Q_3.

VII. SYSTEMATIC UNCERTAINTIES

The dominant systematic uncertainty in this analysis pertains to the unknown spatiotemporal pion distribution at freeze-out on which the fitting of the correlation functions and FSI calculations depends. Typically, a Gaussian profile is assumed in most femtoscopic analyses. However, the known resonances taken all together will generally give rise to non-Gaussian features in the freeze-out distribution.

The systematic uncertainty of the freeze-out distribution is twofold in this analysis. First, it creates an uncertainty in the wave-function integration for the FSI calculation. However, the q dependence of FSI correlations is largely invariant to reasonable variations of the assumed freeze-out distribution and radius. A possible mismatch of the freeze-out distribution and radius in THERMINATOR as compared to the data is largely absorbed by the λ parameter of the global fits to same- and mixed-charge two-pion correlations presented in the Results section. We assign a 2% uncertainty on the two-pion FSI correlations based on the maximum observed difference between FSIs calculated in THERMINATOR and Gaussian particle-emitting source profiles after "rescaling" by an effective λ parameter. We also assign a 2% uncertainty on the r^*-dependent part of the FSI wave functions [26]. Second, the freeze-out distribution uncertainty creates an uncertainty in the fitting of the same-charge correlation functions. A convenient account of sufficiently small deviations from Gaussian behavior in the QS correlation functions can be obtained through an Edgeworth expansion [19]. Deviations from Gaussian behavior are also expected from a finite coherent component [20].

Non-Gaussian features in the QS correlation functions can also occur in more trivial ways. Spherical Gaussian freeze-out distributions create Gaussian QS correlation functions as a function of q. Non-Gaussian features in 1D correlation functions can arise simply from nonequal 3D radii in the LCMS frame. However, we note that $R_{\mathrm{out}} \approx R_{\mathrm{side}}$ and R_{long} is only $\sim$20% larger than R_{out} and R_{side} [15]. Also, k_{T} and centrality bins whose widths are not sufficiently narrow will create a mix of different radii and therefore will not be described by a single Gaussian function. However, our chosen centrality bin width (5%) and k_{T} bin width (100 MeV/c for two-particle correlations) are sufficiently narrow to mostly avoid this feature given the known k_{T} dependencies of the radii [15]. More non-Gaussian features are expected for our three-particle correlations as the k_{T} bin is much wider (1 GeV/c).

The momentum resolution of low-momentum particles ($p_{\mathrm{T}} < 1$ GeV/c) is dominated by multiple scatterings within the ALICE detector. The ALICE material budget uncertainty is conservatively estimated to be $\pm$10%. Our studies suggest a near one-to-one correspondence of the material budget uncertainty with the momentum resolution uncertainty. We apply a 10% uncertainty on all the momentum resolution corrections. For r_3 the momentum resolution correction uncertainty is

found to be 1%. It is not the dominant uncertainty because both numerator and denominator are affected in the same direction.

We study the uncertainties associated with tracking in the ALICE detector in several ways. We study the effect of different magnetic-field orientations in the TPC. The pion particle identification (PID) cuts are tightened by 10%. The angular separation cuts for same-charge pairs are increased by 50%. Positive pions are compared to negative pions. All the uncertainties in this category except for PID were found to be negligible. A 0.3% and 1% systematic uncertainty owing to PID were assigned for three-pion correlation functions and r_3, respectively.

Concerning r_3, additional systematics are included. Imperfect isolation of the three-pion QS cumulant (FSI corrected) is the dominant uncertainty for r_3 which mostly affects the larger values of Q_3 where the cumulant is smallest. The chosen λ parameter ($\lambda = 0.7$) used in extracting the QS correlations in both the numerator and the denominator, while largely canceling in the ratio, is varied by 0.1. Mixed-charge three-pion cumulant correlations ($\mathbf{c}_3^{\pm\pm\mp}$) reveal a slight residual correlation of about 1.005 for all centralities. The residual cumulant correlation in the mixed-charge channel is used as a systematic uncertainty in the same-charge channel. Also, small variations of the powers m and n in Eq. (8) which brought $\mathbf{c}_3^{\pm\pm\mp}$ closer to unity resulted in similar systematic variations for r_3. This procedure is valid if the true FSI-corrected mixed-charge cumulant correlation is expected to be near unity.

The GRS approach to Coulomb corrections is found to give a better description of the mixed-charge correlations than the Ω_0 wave function. For this reason we choose the GRS approach as our principal method and use the Ω_0 wave function as a systematic variation for all three-pion correlations. Finally, nonfemtoscopic background correlations associated with minijets [33], while negligible for the highest multiplicity collisions, create a small uncertainty in the extraction of two-pion QS correlation strengths. A linear fit to the background is made in the interval $0.2 < q < 0.4$ GeV/c and extrapolated into the femtoscopic region, $q < 0.15$ GeV/c. The correction only has a non-negligible effect on r_3 for large Q_3 and above ~40% centrality.

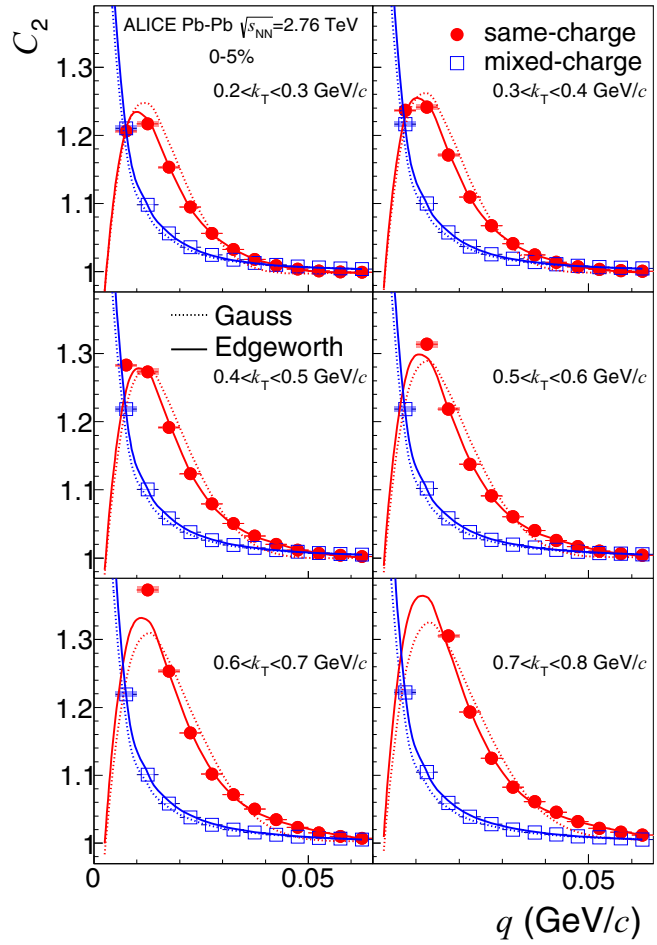

FIG. 2. (Color online) C_2 for same-charge (solid red circles) and mixed-charge pions (open blue squares) for 0%–5% centrality. The global fits with dotted lines correspond to Gaussian same-charge fits ($E_w = 1$). The global fits with solid lines correspond to non-Gaussian fits with Edgeworth coefficients ($E_w \neq 1$). Shaded boxes represent the momentum resolution correction uncertainty. FSI uncertainties are smaller than the symbol sizes.

VIII. RESULTS

A. Two pions

We first present the two-pion correlation functions. Figures 2 and 3 show the same- and mixed-charge correlation functions versus q in 6 k_T bins for 0%–5% and 45%–50% centrality, respectively. Global fits for same and mixed-charge correlations are performed for each k_T bin separately. Two types of global fits are shown. The dotted lines correspond to Gaussian fits ($E_w = 1$), while the solid lines correspond to non-Gaussian fits with Edgeworth coefficients ($E_w \neq 1$). Our strict pair cuts cause a lack of data for same-charge correlations at low q at high k_T, where a larger fraction of the pairs moves collinearly and thus is more susceptible to track merging and splitting.

Concerning the purely Gaussian fits in Figs. 2 and 3, the average χ^2 per degree of freedom (NDF) is 39. It is clear that a spherical Gaussian fully chaotic source can be ruled out. The global fits underestimate mixed-charge correlations for each k_T and centrality bin. The fits indicate the possibility of significant non-Gaussian features in the same-charge correlation functions and/or the possibility of two separate suppression parameters. An individual fit to mixed-charge correlations suggests $\lambda \sim 0.7$. An individual fit to same-charge correlations with a Gaussian function suggests $\lambda \sim 0.4$.

Concerning the Edgeworth fits in Figs. 2 and 3, the average χ^2/NDF is 1.5. Same- and mixed-charge correlations are simultaneously well described with an Edgeworth fit. A common λ parameter is now able to describe both same- and mixed-charge correlations. This may demonstrate the significance of non-Gaussian same-charge correlations and/or the presence of a coherent component.

Fits including coherence with and without the charge constraint were also attempted. The charge constraint on coherent states in the quantum optics [25] approach leads to a slight modification of both same-charge and mixed-charge correlations [20]. It leads to a slight decrease of the suppression

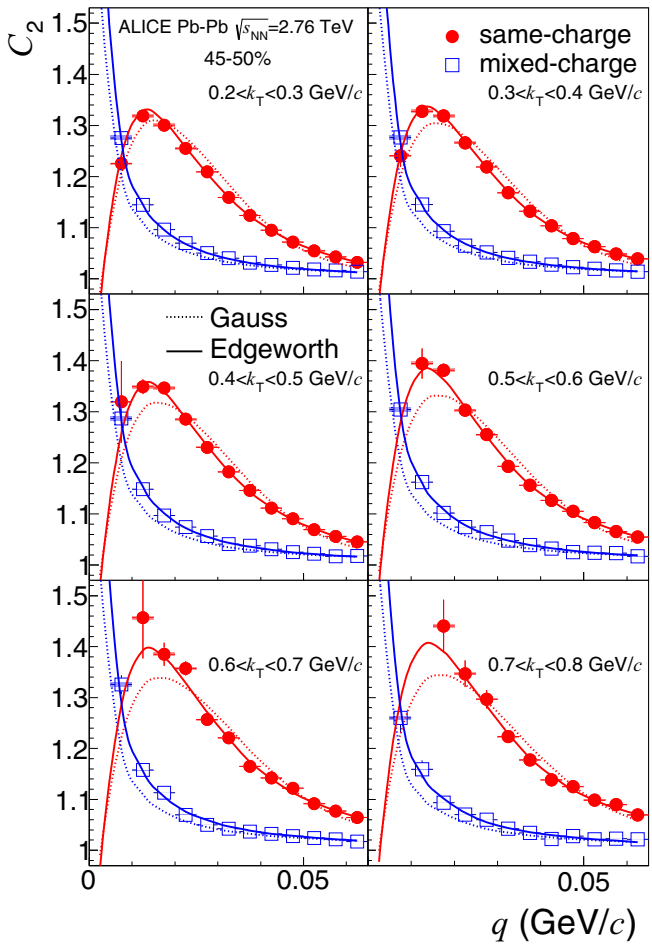

FIG. 3. (Color online) C_2 for same-charge (solid red circles) and mixed-charge pions (open blue squares) for 45%–50% centrality. Same details as for Fig. 2.

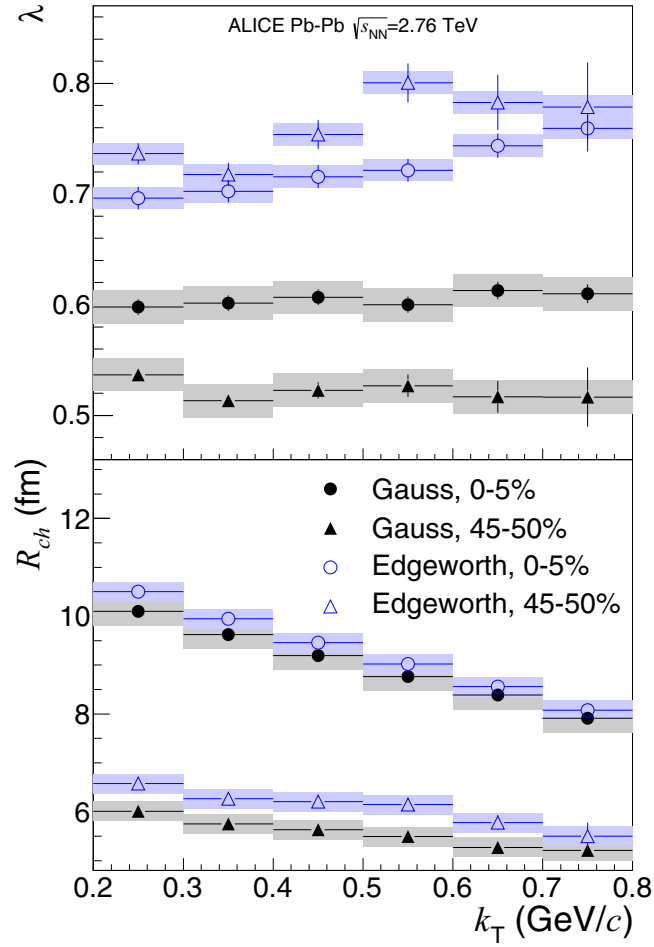

FIG. 4. (Color online) Fit parameters versus k_T for Gaussian and Edgeworth global fits in Figs. 2 and 3. (Top) λ values. (Bottom) R_{ch} values. Shaded bands represent systematic uncertainties.

of same-charge correlations ($\frac{1}{5}G^2$) and also an enhancement of mixed-charge correlations ($\frac{1}{5}G^2$) [20]. Coherence may also explain the observation of separate suppression parameters as it only suppresses same-charge correlations. However, given the uncertainty of non-Gaussian same-charge correlations, we find that two-pion correlations alone are inconclusive in determining the presence of coherence.

The λ and radii fit parameters for both global fit types are shown in Fig. 4. The Edgeworth coefficients from ALICE data are shown in Table I. The corresponding Edgeworth coefficients from THERMINATOR are shown in Table II. The Edgeworth coefficients presented in Tables I and II quantify the non-Gaussian structure of the same-charge correlation functions. They may also be influenced by a coherent component. The comparison of Table I to Table II demonstrates a discrepancy in the shape of QS correlations between THERMINATOR and ALICE data.

The values for the overall normalization, $\mathcal{N}$, are typically within 0.005 from unity. We observe that $\lambda \sim 0.7$ and is largely k_T independent for the Edgeworth fits. The pion-pair purity and the primary-pair purity in this analysis are estimated to be about 93% and 84%, respectively. The correction for muon contamination accounts for pion misidentification. We therefore expect $\lambda < 0.84$. The Gaussian radii are larger than what is typically reported [15] owing to the global fit procedure which incorporates mixed-charge correlations to better constrain the λ parameter. The Edgeworth radii for the chaotic component are observed to be larger than the purely Gaussian radii by ∼10%. We note that it has also been shown that the presence of a finite coherent component can influence the width ($\propto 1/R_{ch}$) of same-charge correlations [2,3,20]. In particular, for the

TABLE I. κ_3 and κ_4 Edgeworth coefficients from ALICE data corresponding to global fits in Figs. 2 and 3. k_{T1} and k_{T6} represent our lowest and highest k_T intervals, respectively.

	k_{T1}	k_{T2}	k_{T3}	k_{T4}	k_{T5}	k_{T6}
κ_3						
0%–5%	0.14	0.13	0.12	0.12	0.1	0.094
45%–50%	0.23	0.22	0.23	0.25	0.25	0.24
κ_4						
0%–5%	0.29	0.33	0.37	0.38	0.43	0.46
45%–50%	0.19	0.22	0.22	0.24	0.25	0.31

TABLE II. κ_3 and κ_4 Edgeworth coefficients from THERMINATOR. k_{T1} and k_{T6} represent our lowest and highest k_T intervals, respectively.

	k_{T1}	k_{T2}	k_{T3}	k_{T4}	k_{T5}	k_{T6}
κ_3						
0%–5%	0.18	0.22	0.27	0.31	0.35	0.4
45%–50%	0.25	0.27	0.3	0.34	0.36	0.42
κ_4						
0%–5%	0.076	0.12	0.17	0.18	0.22	0.23
45%–50%	0.034	0.061	0.081	0.085	0.11	0.084

case when the radius of a coherent component is smaller than the chaotic component, same-charge correlations appear broader than expected by the chaotic component alone. This can incorrectly give the impression of a smaller chaotic source. This may also arise from a momentum dependence of a coherent component (not considered in our fits). For all cases, we observe R_{ch} to decrease with increasing k_T.

A comparison of the k_T evolution of same- and mixed-charge correlations in Figs. 2 and 3 reveals that same-charge correlations change rapidly with increasing k_T while mixed-charge correlations change very little. The widening of same-charge correlations with increasing k_T is potentially caused by radial flow [34,35]. In an expanding source, pairs with large k_T are preferentially formed from particles within the same space-time interval. Thus, larger values of k_T measure smaller lengths of homogeneity. In QS correlations, this will demonstrate itself as a widening of the correlation function with increasing k_T.

Similarly, mixed-charge pairs of larger k_T may also measure smaller lengths of homogeneity owing to radial flow. Mixed-charge correlation strengths may therefore increase with increasing k_T because FSI correlations are larger for smaller sources. In Fig. 5 we present mixed-charge correlations in the form of a ratio, $C_2^{+-}(k_{T6})/C_2^{+-}(k_{T1})$, where k_{T6} and k_{T1} represent our highest (sixth) and lowest (first) k_T bins, respectively. Comparing the ALICE data to the diluted THERMINATOR calculation in Fig. 5, it is clear that the observed mixed-charge correlations evolve less rapidly in real data as compared to the THERMINATOR expectation. This may be caused by a discrepancy of λ or the freeze-out size in THERMINATOR as compared to the data. To distinguish between them, we also compare the ALICE data to the undiluted THERMINATOR calculation in Fig. 5, where only "interacting" pairs with $r^* < 80$ fm are used. Such a procedure can help remove the effect of the λ parameter from the comparison. The k_T evolution of mixed-charge correlations is better described with the undiluted THERMINATOR expectation, which indicates a discrepancy of the k_T evolution of the λ parameter in THERMINATOR as compared to the data.

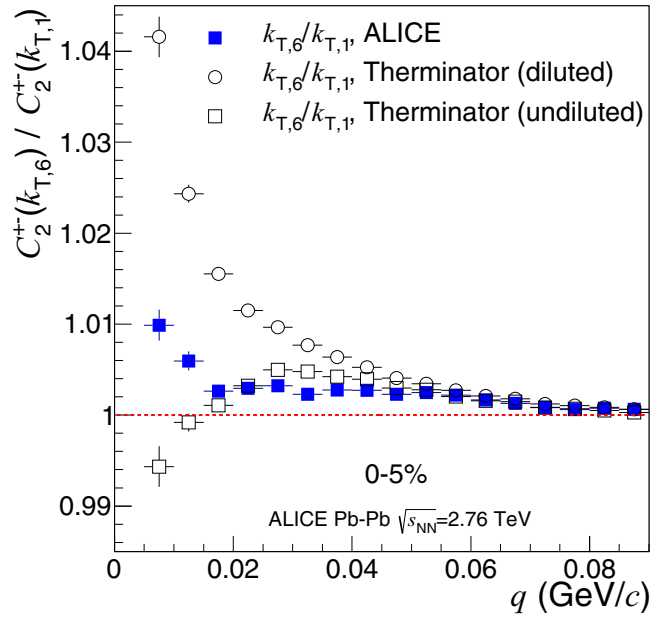

FIG. 5. (Color online) Ratio $C_2^{+-}(k_{T6})/C_2^{+-}(k_{T1})$, comparing mixed-charge correlations between the highest (sixth) and lowest (first) k_T bins. Open circles represent the THERMINATOR comparison using all pion pairs (diluted). Open squares represent the THERMINATOR calculation only using pion pairs with $r^* < 80$ fm (undiluted). Error bars include statistical and systematic uncertainties.

B. Three pions

We now present the three-pion same- and mixed-charge correlation functions in two $K_{T,3} = |\mathbf{p}_{T,1} + \mathbf{p}_{T,2} + \mathbf{p}_{T,3}|/3$ bins. Two $K_{T,3}$ intervals were chosen such that they divide the number of triplets into two roughly equal halves. The same-charge three-pion correlations in six centrality bins and two $K_{T,3}$ bins are shown in Figs. 6 and 7. Also shown are the cumulant correlation functions, $\mathbf{c}_3$, for which the two-pion correlations and FSIs are removed. The dilution of correlations caused by $\lambda < 1$ is also removed when we consider $\mathbf{c}_3$. Extraction of the cumulant correlation function, $\mathbf{c}_3$, requires an assumption on the λ parameter. We use the λ parameter obtained from two-pion global fits excluding coherence and incorporating an Edgeworth expansion to the full k_T range ($0 < k_T < 1.0$). From central to peripheral collisions, λ ranges from 0.65 to 0.70. In Figs. 6 and 7 we observe that the raw same-charge three-pion correlations are suppressed far below the expected value for fully chaotic emission [$C_3^{\pm\pm\pm}(Q_3 = 0) < 6$] as was similarly seen for $C_2^{\pm\pm}$. The same-charge cumulant correlation also appears to be suppressed below its maximum [$\mathbf{c}_3(Q_3 = 0) < 3$] although a reliable extrapolation to $Q_3 = 0$ is needed to be sure.

The mixed-charge three-pion correlations and cumulant correlations in six centrality bins and two $K_{T,3}$ bins are shown in Figs. 8 and 9. For mixed-charge correlations, $\mathbf{c}_3^{\pm\pm\mp}$ is expected to be equal to unity in the presence of only QS and FSIs. The construction of the cumulant correlation function removes FSI effects and the dilution when $\lambda < 1$. The mixed-charge cumulant correlation is largely consistent with unity for both $K_{T,3}$ bins although the positive residue for the highest $K_{T,3}$ bin is about 2 times larger than for the lowest bin. This demonstrates the validity of asymptotic three-body FSI wave functions for Pb-Pb collisions at the LHC for $Q_3 > 10$ MeV/c. We note that it may also be possible for a residue to exist for $\mathbf{c}_3^{\pm\pm\mp}$ with charge-constrained coherent states [20]. The cumulant correlation functions in Figs. 8

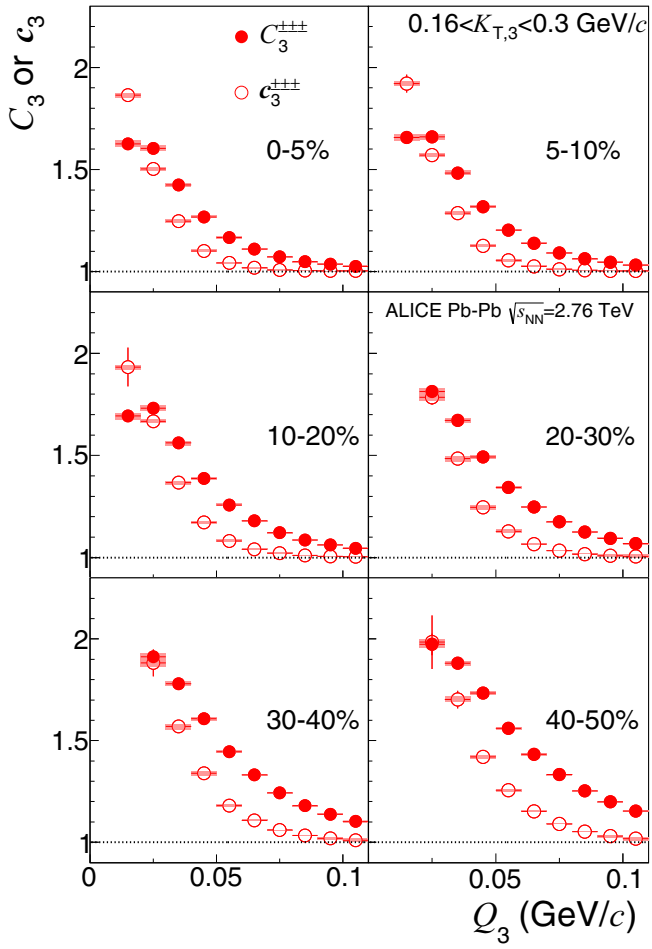

FIG. 6. (Color online) Same-charge C_3 (solid red circles) for each centrality bin for $0.16 < K_{T,3} < 0.3$ GeV/c. Open points represent the corresponding cumulant correlation functions, $\mathbf{c}_3$. Shaded bands represent systematic uncertainties.

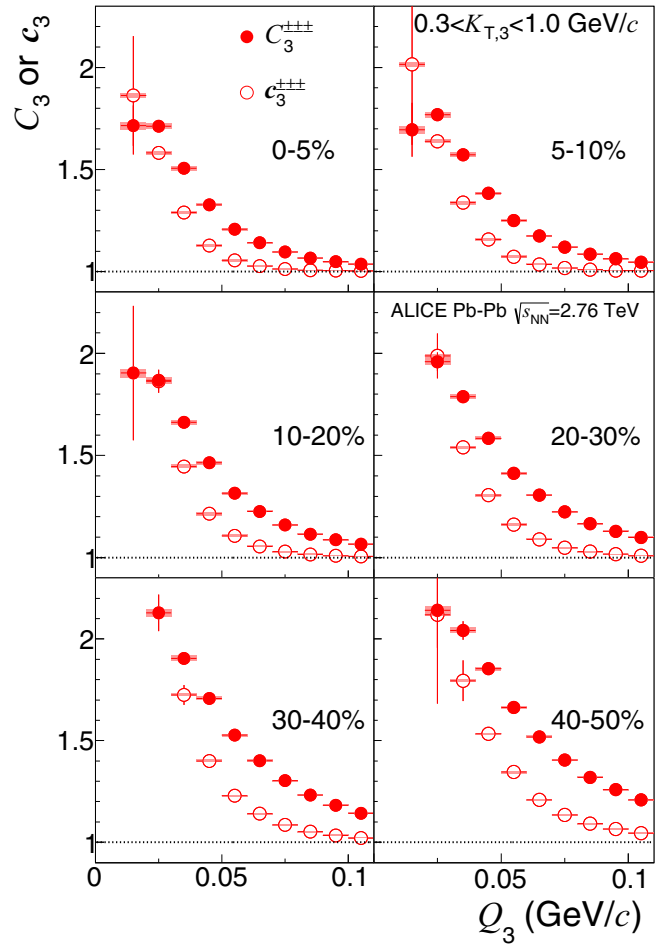

FIG. 7. (Color online) Same-charge C_3 (solid red circles) for each centrality bin for $0.3 < K_{T,3} < 1.0$ GeV/c. Same details as for Fig. 6.

and 9 suggest a residual correlation less than about 1.005. The removal of FSI effects is crucial for the interpretation of the intercept of r_3. The successful removal of FSI effects in the mixed-charge three-pion system is demonstrated with the cumulant correlation function in Figs. 8 and 9.

The three-pion QS cumulant is compared to the two-pion QS cumulant with r_3. Unlike fits at the two-particle level alone, the intercept of r_3 is more robust to non-Gaussian QS correlations. By construction, $r_3(Q_3 = 0) = 2.0$ in the absence of coherence regardless of the shape of QS correlations [21]. To leading order, the relative momentum dependence of r_3 was shown to be quartic in the full 6D approach [21]. However, owing to limited statistical precision we project r_3 onto 1D Q_3.

We now present r_3 versus Q_3 in Figs. 10 and 11 in six centrality bins and two $K_{T,3}$ bins. The data are fit with a quartic and quadratic fit as shown by Eqs. (11) and (12). The systematic uncertainties at large Q_3 are typically larger than 50%, while at low Q_3 they are much smaller. At low Q_3, one notices that r_3 is further below the chaotic limit (2.0) in Fig. 10 than in Fig. 11.

The largest systematic uncertainty in Figs. 10 and 11 is attributable to the residual correlation of $\mathbf{c}_3^{\pm\pm\mp}$. The systematic uncertainties are larger for the higher $K_{T,3}$ bin owing to a larger residual correlation of $\mathbf{c}_3^{\pm\pm\mp}$. The dashed black lines in Figs. 10 and 11 represent the systematic uncertainty owing to FSI corrections. It is estimated by the difference in Ω_0 and GRS FSI calculations as was illustrated in Fig. 1. Figure 12 compares the effect of both FSI corrections on r_3 and $\mathbf{c}_3^{\pm\pm\mp}$. From the top panel of Fig. 12 we see that the Ω_0 FSI correction procedure yields an intercept closer to the chaotic limit than the GRS procedure. However, from the bottom panel of Fig. 12 we see that a large unexplained residual spike remains with the Ω_0 FSI correction procedure. For this reason the GRS procedure was chosen as our standard. We have also investigated other source profile integrations where one obtains larger FSI correlations. Such variations, which bring the intercept of r_3 to the chaotic limit, simultaneously cause a large overcorrection of the mixed-charge three-pion cumulant, $\mathbf{c}_3^{\pm\pm\mp}(Q_3 \sim 0) \sim 0.96$.

In Fig. 13 we show r_3 with two different assumptions on the λ parameter. The default value of 0.7 is compared to 0.6 in Fig. 13. The default value was motivated by Edgeworth fits

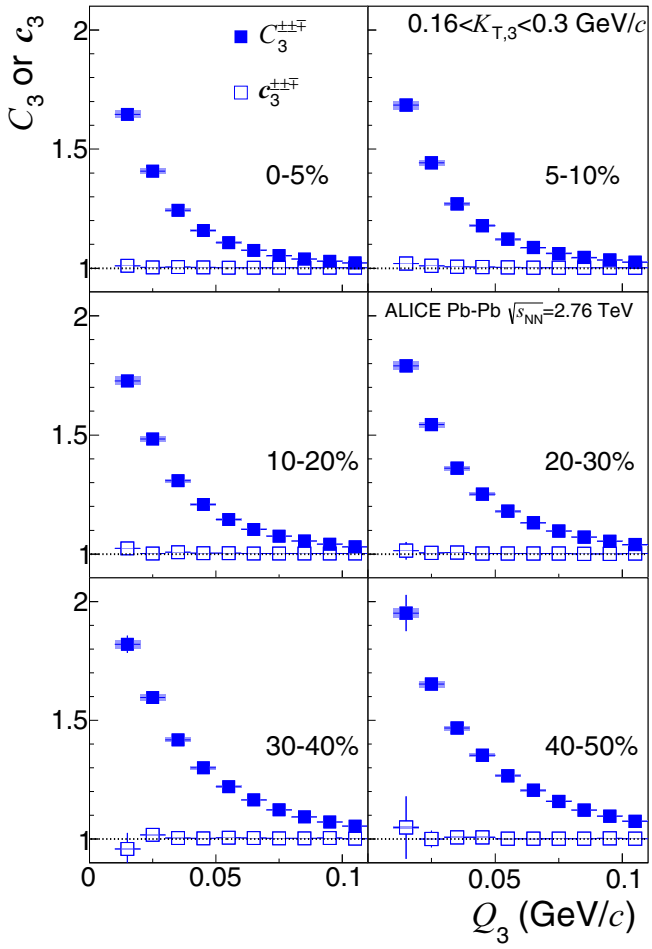

FIG. 8. (Color online) Mixed-charge C_3 (solid blue squares) for each centrality bin for $0.16 < K_{T,3} < 0.3$ GeV/c. Open squares represent the corresponding cumulant correlation functions, $\mathbf{c}_3$. Shaded bands represent systematic uncertainties.

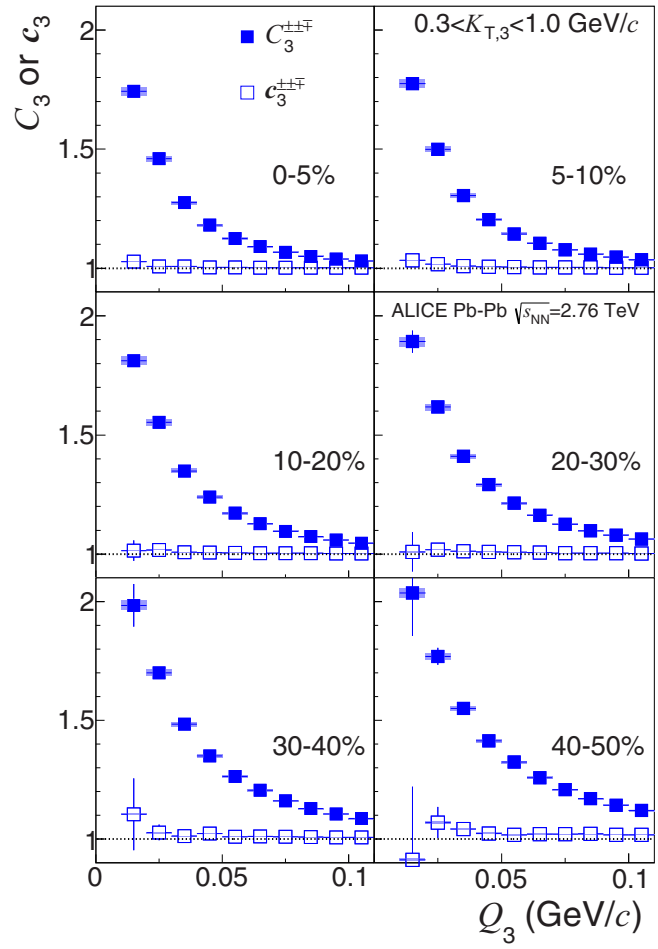

FIG. 9. (Color online) Mixed-charge C_3 (solid blue squares) for each centrality bin for $0.3 < K_{T,3} < 1.0$ GeV/c. Same details as for Fig. 8.

at the two-pion level as was shown in Fig. 4. The effect of the chosen λ parameter only has non-negligible effect at large Q_3 and in central collisions where the cumulant correlation is small, $\mathbf{c}_3^{\pm\pm\pm} \sim 1.0$.

We see that the Q_3 dependence of r_3 is largely uncertain for the more central collisions. This is caused by the uncertainty in isolating the three-pion QS cumulant when the cumulant correlation itself is small, $\mathbf{c}_3^{\pm\pm\pm} \sim 1.0$. A quartic [Eq. (11)] and quadratic [Eq. (12)] fit are shown in Figs. 10 and 11 and are summarized in Tables III and IV, respectively.

Given the large uncertainties at large Q_3, r_3 does not change significantly with centrality and is equally well described by quartic and quadratic fits. The centrality averaged fit values are also given in Tables III and IV.

From the intercepts of r_3 at $Q_3 = 0$ presented in Tables III and IV, the corresponding coherent fractions (G) may be extracted using Eq. (13). For low $K_{T,3}$, the centrality averaged intercepts (0%–50%) of r_3 may correspond to coherent fractions of 28% ± 3% and 24% ± 9% for quartic and quadratic intercepts, respectively. For high $K_{T,3}$, the corresponding coherent fractions are consistent with zero for both quartic and

TABLE III. Quartic r_3 fit parameters from Figs. 10 and 11. The centrality averaged values are also shown. Statistical and systematic uncertainties are shown. Low $K_{T,3}$ refers to $0.16 < K_{T,3} < 0.3$ GeV/c. High $K_{T,3}$ refers to $0.3 < K_{T,3} < 1.0$ GeV/c.

	$I \pm$ stat $\pm$ syst	$a \times 10^3$ (GeV/c)$^{-4}$
Low $K_{T,3}$		
0%–5%	$1.84 \pm 0.01 \pm 0.03$	$3.0 \pm 0.6 \pm 16.4$
5%–10%	$1.85 \pm 0.01 \pm 0.05$	$3.4 \pm 0.7 \pm 13.0$
10%–20%	$1.84 \pm 0.02 \pm 0.03$	$2.4 \pm 0.9 \pm 8.1$
20%–30%	$1.86 \pm 0.03 \pm 0.01$	$4.6 \pm 1.0 \pm 3.7$
30%–40%	$1.82 \pm 0.04 \pm 0.03$	$2.7 \pm 1.3 \pm 2.8$
40%–50%	$1.77 \pm 0.05 \pm 0.01$	$4.8 \pm 1.6 \pm 1.1$
0%–50%	$1.83 \pm 0.01 \pm 0.03$	$3.5 \pm 0.4 \pm 7.5$
High $K_{T,3}$		
0%–5%	$1.95 \pm 0.02 \pm 0.02$	$0.5 \pm 0.7 \pm 10.1$
5%–10%	$1.93 \pm 0.02 \pm 0.01$	$-1.8 \pm 0.8 \pm 8.4$
10%–20%	$2.06 \pm 0.03 \pm 0.07$	$2.3 \pm 1.1 \pm 5.7$
20%–30%	$2.01 \pm 0.04 \pm 0.01$	$0.0 \pm 1.3 \pm 3.0$
30%–40%	$2.04 \pm 0.06 \pm 0.05$	$-0.2 \pm 1.8 \pm 3.0$
40%–50%	$2.04 \pm 0.09 \pm 0.04$	$-2.6 \pm 2.4 \pm 1.4$
0%–50%	$2.00 \pm 0.02 \pm 0.03$	$-0.3 \pm 0.6 \pm 5.3$

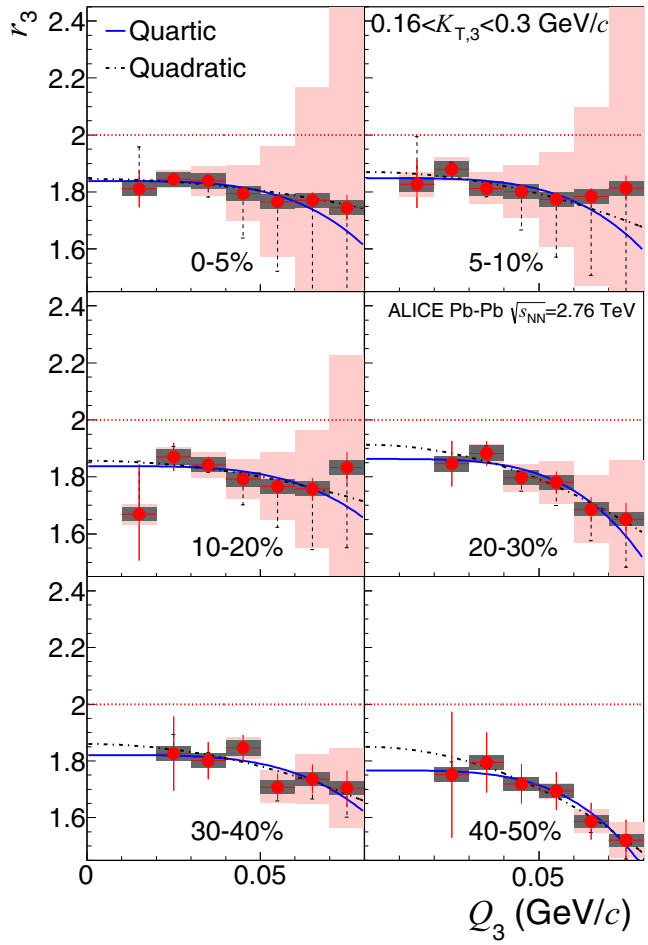

FIG. 10. (Color online) r_3 versus Q_3 in six centrality bins for $0.16 < K_{T,3} < 0.3$ GeV/c. r_3 was measured in 5% centrality widths and averaged over the total bin width. The blue solid line is a quartic fit [Eq. (11)] and the dashed black line is a quadratic fit [Eq. (12)]. The chaotic upper limit [$r_3(Q_3) = 2$] is shown with the dashed red line. The shaded gray band represents the systematics owing to PID and momentum resolution. The shaded red band represents the uncertainties owing to the choice of λ and the residue of the mixed-charge cumulant correlations. The dashed line represents uncertainties on the FSI corrections.

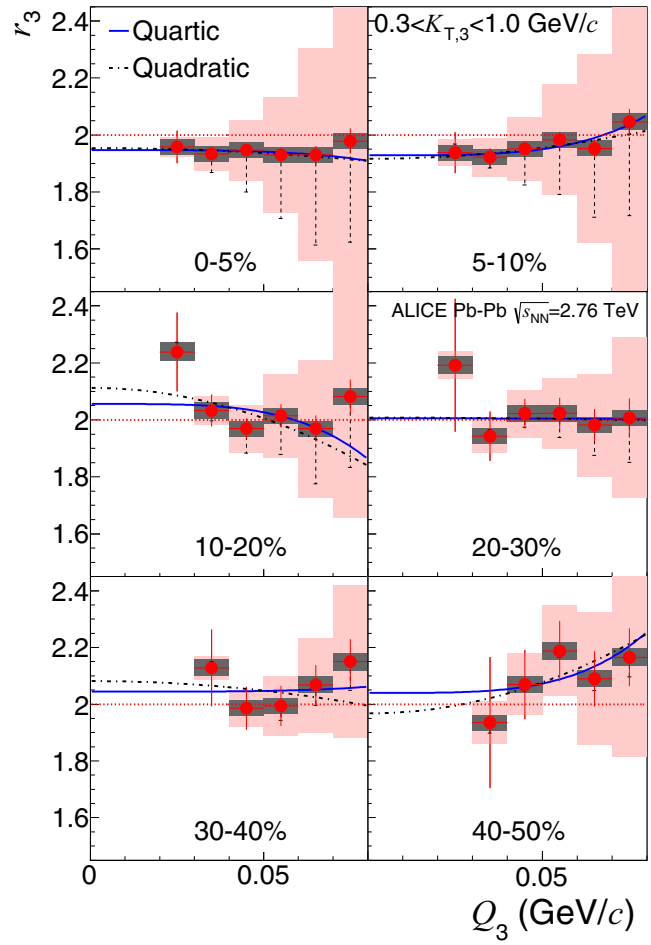

FIG. 11. (Color online) r_3 versus Q_3 in six centrality bins for $0.3 < K_{T,3} < 1.0$ GeV/c. Same details as in Fig. 10.

quadratic fits. Given the systematic uncertainties at large Q_3, both quartic and quadratic fits provide a good description of r_3. We estimate the average coherent fraction at low $K_{T,3}$ using both quartic and quadratic fits as well as their uncertainties as $(G^{\text{quartic}} + \delta G^{\text{quartic}} + G^{\text{quadratic}} - \delta G^{\text{quadratic}})/2$. The average coherent fraction at low $K_{T,3}$ is estimated to be $23\% \pm 8\%$.

As a sanity check, we also reconstructed r_3 in HIJING including the simulated response of the ALICE detector. HIJING does not contain QS nor FSIs. We used a known symmetric and fully chaotic QS + FSI correlation as a pair/triplet fill weight. The same code developed for this analysis was used in this procedure. The reconstructed r_3 for both $K_{T,3}$ bins was consistent with the chaotic limit for all Q_3.

TABLE IV. Quadratic r_3 fit parameters from Figs. 10 and 11. The centrality averaged values are also shown. Statistical and systematic uncertainties are shown. Low $K_{T,3}$ refers to $0.16 < K_{T,3} < 0.3$ GeV/c. High $K_{T,3}$ refers to $0.3 < K_{T,3} < 1.0$ GeV/c.

	$I \pm \text{stat} \pm \text{syst}$	$a \times 10^1$ (GeV/c)$^{-2}$
Low $K_{T,3}$		
0%–5%	$1.85 \pm 0.02 \pm 0.11$	$0.9 \pm 0.3 \pm 6.7$
5%–10%	$1.87 \pm 0.02 \pm 0.12$	$1.6 \pm 0.4 \pm 5.8$
10%–20%	$1.86 \pm 0.03 \pm 0.09$	$1.2 \pm 0.5 \pm 4.1$
20%–30%	$1.91 \pm 0.04 \pm 0.04$	$2.5 \pm 0.6 \pm 1.9$
30%–40%	$1.86 \pm 0.05 \pm 0.07$	$1.7 \pm 0.8 \pm 1.7$
40%–50%	$1.85 \pm 0.08 \pm 0.01$	$3.2 \pm 1.0 \pm 0.7$
0%–50%	$1.87 \pm 0.02 \pm 0.07$	$1.8 \pm 0.3 \pm 3.5$
High $K_{T,3}$		
0%–5%	$1.95 \pm 0.03 \pm 0.06$	$0.4 \pm 0.5 \pm 4.8$
5%–10%	$1.92 \pm 0.03 \pm 0.07$	$-0.8 \pm 0.5 \pm 4.4$
10%–20%	$2.11 \pm 0.05 \pm 0.12$	$2.0 \pm 0.7 \pm 3.5$
20%–30%	$2.01 \pm 0.07 \pm 0.05$	$0.1 \pm 0.9 \pm 1.9$
30%–40%	$2.08 \pm 0.09 \pm 0.13$	$0.6 \pm 1.3 \pm 2.4$
40%–50%	$1.97 \pm 0.15 \pm 0.07$	$-2.2 \pm 1.9 \pm 1.1$
0%–50%	$2.01 \pm 0.03 \pm 0.08$	$0.0 \pm 0.5 \pm 3.0$

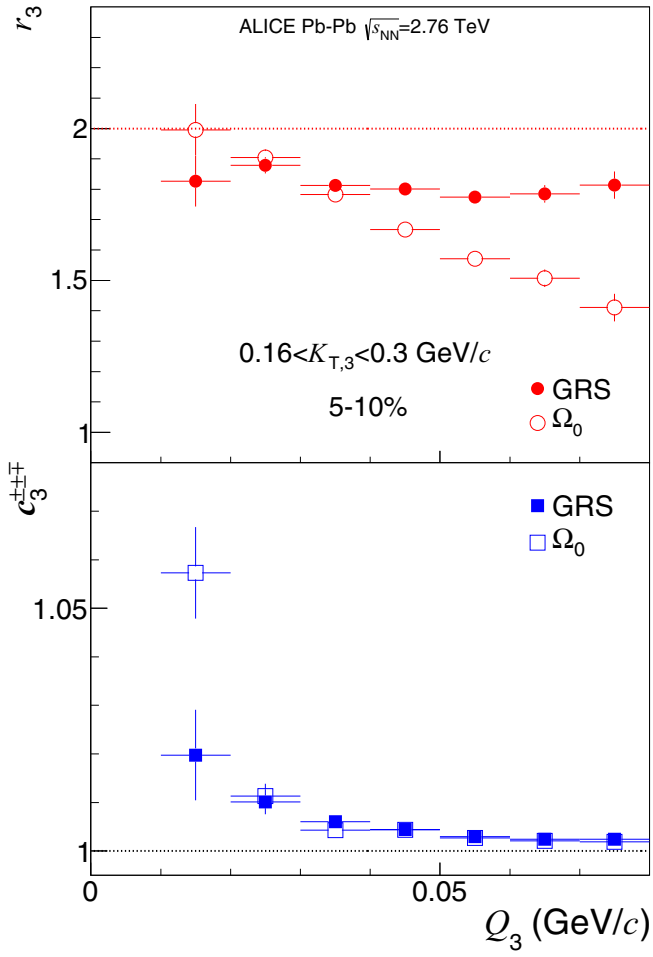

FIG. 12. (Color online) In the top panel, r_3 versus Q_3 is shown with GRS and Ω_0 FSI corrections. In the bottom panel, $\mathbf{c}_3^{\pm\pm\mp}$ versus Q_3 is shown with both FSI corrections. The centrality and $K_{T,3}$ interval is 5%–10% centrality and $0.16 < K_{T,3} < 0.3$ GeV/c, respectively. Only statistical errors are shown for clarity.

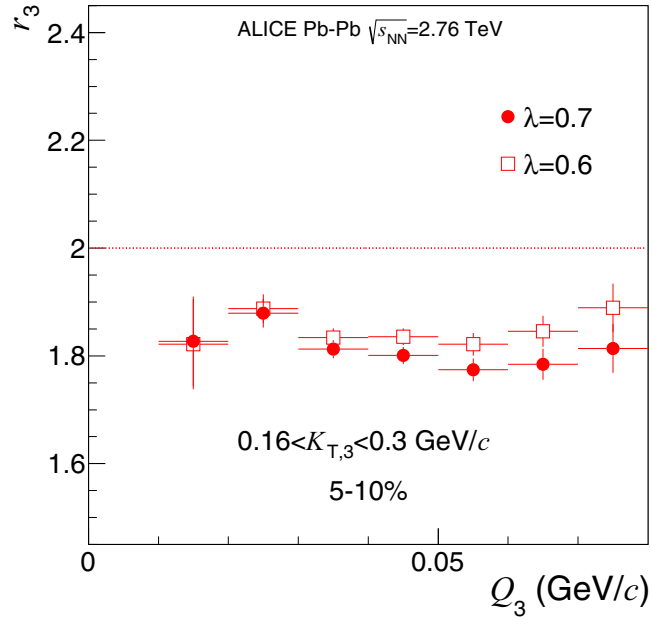

FIG. 13. (Color online) r_3 versus Q_3 is shown with two different assumptions on the λ parameter for 5%–10% centrality and for $0.16 < K_{T,3} < 0.3$ GeV/c. Only statistical errors are shown for clarity.

IX. CONCLUSIONS

Two- and three-pion quantum statistical correlations in Pb-Pb collisions at $\sqrt{s_{NN}} = 2.76$ TeV have been presented. Same-charge as well as mixed-charge combinations were shown for both two- and three-pion correlations. While same-charge correlations uniquely display the effect of quantum interference, mixed-charge correlations provide an important constraint on the λ parameter and FSI corrections in this analysis.

At the two-pion level, we find that while same-charge correlations change rapidly with k_T, mixed-charge correlations change very little. A comparison of mixed-charge correlations to THERMINATOR suggests that the λ parameter changes very little with k_T. Global fits to same- and mixed-charge correlations at the two-pion level alone are inconclusive in determining the presence of coherence owing to the unknown non-Gaussian features of the same-charge correlation function.

Three-pion mixed-charge correlations are very well described by the combination of QS and FSI correlations. While the mixed-charge three-pion cumulant correlation is largely consistent with unity, the same-charge three-pion cumulant shows a significant QS correlation.

The comparison of the three-pion cumulant to the two-pion cumulant is measured with r_3. Unlike fits at the two-pion level alone, the intercept of r_3 is more robust to non-Gaussian Bose-Einstein correlations. We find a clear suppression of r_3 below the chaotic limit for low $K_{T,3}$ while being much more consistent with the chaotic limit for high $K_{T,3}$. Incomplete FSI removal, momentum resolution correction, and pion misidentification can also cause an apparent suppression of r_3. However, the $K_{T,3}$ dependencies of the r_3 intercepts go in the opposite direction than would be expected from such effects .

Given the large uncertainties at large Q_3, r_3 does not change significantly with centrality. For low triplet momentum, the centrality averaged intercepts of r_3 may correspond to a coherent fraction of $23\% \pm 8\%$. For high triplet momentum the intercepts of r_3 yield a coherent fraction consistent with zero.

The suppression of three-pion as compared to two-pion Bose-Einstein correlations as measured by r_3 seems to suggest a finite coherent component to pion production in heavy-ion collisions. It is significant at low triplet momentum while vanishing for high triplet momentum. This observation is qualitatively consistent with the formation of a Bose-Einstein condensate which is expected to radiate coherently at low momentum. More experimental and theoretical work is needed to rule out alternative explanations. Other measurements such as the single-pion spectra should provide additional information on this subject. We also note that the ALICE single-pion spectra indicate a small excess of pion production as compared to several hydrodynamic calculations for $p_T < 0.4$ GeV/c [36]. The mean p_T of pions for low Q_3 in our

lowest and highest $K_{T,3}$ bin is about 0.24 and 0.38 GeV/c, respectively. The excess in the single-pion spectra may be related to the coherent fractions extracted in this analysis.

ACKNOWLEDGMENTS

We would like to thank Richard Lednický, Ulrich Heinz, Tamás Csörgő, Máté Csanád, and Yuri Sinyukov for numerous helpful discussions. The ALICE collaboration would like to thank all its engineers and technicians for their invaluable contributions to the construction of the experiment and the CERN accelerator teams for the outstanding performance of the LHC complex. The ALICE collaboration gratefully acknowledges the resources and support provided by all Grid centers and the Worldwide LHC Computing Grid (WLCG) collaboration. The ALICE collaboration acknowledges the following funding agencies for their support in building and running the ALICE detector: State Committee of Science, World Federation of Scientists (WFS), and Swiss Fonds Kidagan, Armenia, Conselho Nacional de Desenvolvimento Científico e Tecnológico (CNPq), Financiadora de Estudos e Projetos (FINEP), Fundação de Amparo à Pesquisa do Estado de São Paulo (FAPESP); National Natural Science Foundation of China (NSFC), the Chinese Ministry of Education (CMOE), and the Ministry of Science and Technology of China (MSTC); Ministry of Education and Youth of the Czech Republic; Danish Natural Science Research Council, the Carlsberg Foundation, and the Danish National Research Foundation; The European Research Council under the European Community's Seventh Framework Programme; Helsinki Institute of Physics and the Academy of Finland; French Grant No. CNRS-IN2P3, the "Region Pays de Loire," "Region Alsace," "Region Auvergne," and CEA, France; German BMBF and the Helmholtz Association; General Secretariat for Research and Technology, Ministry of Development, Greece; Hungarian OTKA and National Office for Research and Technology (NKTH); Department of Atomic Energy and Department of Science and Technology of the Government of India; Istituto Nazionale di Fisica Nucleare (INFN) and Centro Fermi-Museo Storico della Fisica e Centro Studi e Ricerche "Enrico Fermi," Italy; MEXT Grant-in-Aid for Specially Promoted Research, Japan; Joint Institute for Nuclear Research, Dubna; National Research Foundation of Korea (NRF); CONACYT, DGAPA, México; ALFA-EC and the EPLANET Program (European Particle Physics Latin American Network) Stichting voor Fundamenteel Onderzoek der Materie (FOM) and the Nederlandse Organisatie voor Wetenschappelijk Onderzoek (NWO), Netherlands; Research Council of Norway (NFR); Polish Ministry of Science and Higher Education and National Science Centre, Poland; Ministry of National Education/Institute for Atomic Physics and CNCS-UEFISCDI, Romania; Ministry of Education and Science of Russian Federation, Russian Academy of Sciences, Russian Federal Agency of Atomic Energy, Russian Federal Agency for Science and Innovations, and The Russian Foundation for Basic Research; Ministry of Education of Slovakia; Department of Science and Technology, South Africa; CIEMAT, EELA, Ministerio de Economía y Competitividad (MINECO) of Spain; Xunta de Galicia (Consellería de Educación), CEADEN, Cubaenergía, Cuba; IAEA (International Atomic Energy Agency); Swedish Research Council (VR) and Knut & Alice Wallenberg Foundation (KAW); Ukraine Ministry of Education and Science; United Kingdom Science and Technology Facilities Council (STFC); The United States Department of Energy, the United States National Science Foundation, the State of Texas, and the State of Ohio.

APPENDIX: RELATION OF N_3 TO N_3^{QS}

The measurement of the true three-pion correlation is more involved when the "dilution" parameter, λ, is less than unity. In the core/halo picture [37], the effective intercept parameter is given by λ_* which represents the fraction of pairs interacting at low relative momentum via QS + FSIs above the resolvable threshold q_{min}. Here, λ includes the additional dilution caused by secondary contamination and pion mis-identification. The probability of choosing N particles from the interacting core is $\lambda^{N/2}$. In general, λ is less than unity. This means that despite measuring three pions from the same event, there will be a fraction of triplets which do not represent a true three-particle interaction. These feed-up contributions must be removed. In general, the measured three-particle distribution will take on the form

$$\begin{aligned} &N_3(p_1,p_2,p_3)\\ &\quad= f_1' N_1(p_1)N_1(p_2)N_1(p_3) + f_2'\big[N_2^{\mathrm{true}}(p_1,p_2)N_1(p_3)\\ &\qquad + N_2^{\mathrm{true}}(p_3,p_1)N_1(p_2) + N_2^{\mathrm{true}}(p_2,p_3)N_1(p_1)\big]\\ &\qquad + f_3' N_3^{\mathrm{true}}(p_1,p_2,p_3), \end{aligned} \tag{A1}$$

where f_1', f_2', f_3' represent the fraction of triplets for which none interact, two interact, and all three interact, respectively. The probability that all three are from the noninteracting halo is then $(1-\lambda^{1/2})^3$. The probability that only one is from the interacting core is $3\lambda^{1/2}(1-\lambda^{1/2})^2$. Therefore,

$$f_1' = (1-\lambda^{1/2})^3 + 3\lambda^{1/2}(1-\lambda^{1/2})^2. \tag{A2}$$

The probability that two are from the interacting core is $\lambda(1-\lambda^{1/2})$. Therefore,

$$f_2' = \lambda(1-\lambda^{1/2}). \tag{A3}$$

Finally, the probability that all three are from the interacting core is $\lambda^{3/2}$. Therefore,

$$f_3' = \lambda^{3/2}. \tag{A4}$$

Now we can write the equation expressing the triplet distribution in terms of the true distributions:

$$\begin{aligned} &N_3(p_1,p_2,p_3)\\ &\quad= [(1-\lambda^{1/2})^3 + 3\lambda^{1/2}(1-\lambda^{1/2})^2]N_1(p_1)N_1(p_2)N_1(p_3)\\ &\qquad + \lambda(1-\lambda^{1/2})\big[N_2^{\mathrm{true}}(p_1,p_2)N_1(p_3)\\ &\qquad + N_2^{\mathrm{true}}(p_3,p_1)N_1(p_2) + N_2^{\mathrm{true}}(p_2,p_3)N_1(p_1)\big]\\ &\qquad + \lambda^{3/2}N_3^{\mathrm{true}}(p_1,p_2,p_3). \end{aligned} \tag{A5}$$

N_2^{true} is related to the measured N_2 through Eq. (2) with $\mathcal{N}=1$. Finally, we assume a factorization of the three-pion FSI correlation, K_3, from the QS correlation. We can now

form a relation between the QS three-pion distribution and the measured distributions:

$$N_3(p_1,p_2,p_3) = [(1-\lambda^{1/2})^3 + 3\lambda^{1/2}(1-\lambda^{1/2})^2 - 3(1-\lambda^{1/2})(1-\lambda)]N_1(p_1)N_1(p_2)N_1(p_3) + (1-\lambda^{1/2})[N_2(p_1,p_2)N_1(p_3) + N_2(p_3,p_1)N_1(p_2) + N_2(p_2,p_3)N_1(p_1)] + \lambda^{3/2}K_3N_3^{\mathrm{QS}}(p_1,p_2,p_3). \quad \text{(A6)}$$

[1] G. Goldhaber, S. Goldhaber, W. Y. Lee, and A. Pais, Phys. Rev. **120**, 300 (1960).
[2] G. N. Fowler and R. M. Weiner, Phys. Rev. D **17**, 3118 (1978).
[3] M. Gyulassy, S. K. Kauffmann, and L. W. Wilson, Phys. Rev. C **20**, 2267 (1979).
[4] G. N. Fowler, N. Stelte, and R. M. Weiner, Nucl. Phys. A **319**, 349 (1979).
[5] J. D. Bjorken, K. L. Kowalski, and C. C. Taylor, SLAC-PUB-6109, 1993.
[6] L. McLerran and R. Venugopalan, Phys. Rev. D **49**, 3352 (1994); **49**, 2233 (1994).
[7] J. P. Blaizot *et al.*, Nucl. Phys. A **873**, 68 (2012).
[8] H. Boggild *et al.* (NA44 Collaboration), Phys. Lett. B **455**, 77 (1999); I. G. Bearden *et al.* (NA44 Collaboration), *ibid.* **517**, 25 (2001).
[9] M. M. Aggarwal *et al.* (WA98 Collaboration), Phys. Rev. Lett. **85**, 2895 (2000).
[10] J. Adams *et al.* (STAR Collaboration), Phys. Rev. Lett. **91**, 262301 (2003).
[11] K. Aamodt *et al.* (ALICE Collaboration), JINST **3**, S08002 (2008).
[12] B. Abelev *et al.* (ALICE Collaboration), Phys. Rev. C **88**, 044909 (2013).
[13] K. Aamodt *et al.* (ALICE Collaboration), Phys. Rev. Lett. **105**, 252301 (2010).
[14] J. Alme *et al.* (ALICE Collaboration), Nucl. Instrum. Meth. A **622**, 316 (2010).
[15] K. Aamodt *et al.* (ALICE Collaboration), Phys. Lett. B **696**, 328 (2011).
[16] J. Adams *et al.* (STAR Collaboration), Phys. Rev. C **71**, 044906 (2005).
[17] M. G. Bowler, Phys. Lett. B. **270**, 69 (1991).
[18] Yu. M. Sinyukov *et al.*, Phys. Lett. B **432**, 249 (1998).
[19] T. Csorgo and S. Hegyi, Phys. Lett. B **489**, 15 (2000).
[20] S. V. Akkelin, R. Lednicky, and Yu. M. Sinyukov, Phys. Rev. C **65**, 064904 (2002).
[21] U. Heinz and Q. H. Zhang, Phys. Rev. C **56**, 426 (1997).
[22] U. Heinz and A. Sugarbaker, Phys. Rev. C **70**, 054908 (2004).
[23] J. C. Botke, D. J. Scalapino, and R. L. Sugar, Phys. Rev. D **9**, 813 (1974).
[24] M. Biyajima, A. Ohsawa, N. Suzuki, and I. V. Andreev, Phys. Rev. C **58**, 2316 (1998).
[25] R. J. Glauber, Phys. Rev. **130**, 2529 (1963); **131**, 2766 (1963).
[26] R. Lednicky, Phys. Part. Nucl. **40**, 307 (2009).
[27] A. Kisiel, T. Taluc, W. Broniowski, and W. Florkowski, Comput. Phys. Commun. **174**, 669 (2006).
[28] P. Bozek, Phys. Rev. C **77**, 034911 (2008).
[29] E. O. Alt and A. M. Mukhamedzhanov, Phys. Rev. A **47**, 2004 (1993).
[30] E. O. Alt *et al.*, Phys. Lett. B **458**, 407 (1999).
[31] Y. M. Liu, D. Beavis, S. Y. Chu, S. Y. Fung, D. Keane, G. Van Dalen, and M. Vient, Phys. Rev. C **34**, 1667 (1986).
[32] M. Gyulassy and X. N. Wang, Comput. Phys. Commun. **83**, 307 (1994); X. N. Wang and M. Gyulassy, Phys. Rev. D **44**, 3501 (1991).
[33] K. Aamodt *et al.* (ALICE Collaboration), Phys. Rev. D **84**, 112004 (2011).
[34] S. Pratt, Phys. Rev. Lett. **53**, 1219 (1984).
[35] A. N. Makhlin and Y. M. Sinyukov, Z. Phys. C **39**, 69 (1988).
[36] B. Abelev *et al.* (ALICE Collaboration), Phys. Rev. C **88**, 044910 (2013).
[37] T. Csorgo, B. Lorstad, and J. Zimanyi, Z. Phys. C **71**, 491 (1996).

B. Abelev,[1] J. Adam,[2] D. Adamová,[3] M. M. Aggarwal,[4] G. Aglieri Rinella,[5] M. Agnello,[6,7] A. G. Agocs,[8] A. Agostinelli,[9] N. Agrawal,[10] Z. Ahammed,[11] N. Ahmad,[12] A. Ahmad Masoodi,[12] I. Ahmed,[13] S. U. Ahn,[14] S. A. Ahn,[14] I. Aimo,[6,7] S. Aiola,[15] M. Ajaz,[13] A. Akindinov,[16] D. Aleksandrov,[17] B. Alessandro,[7] D. Alexandre,[18] A. Alici,[19,20] A. Alkin,[21] J. Alme,[22] T. Alt,[23] V. Altini,[24] S. Altinpinar,[25] I. Altsybeev,[26] C. Alves Garcia Prado,[27] C. Andrei,[28] A. Andronic,[29] V. Anguelov,[30] J. Anielski,[31] T. Antičić,[32] F. Antinori,[33] P. Antonioli,[20] L. Aphecetche,[34] H. Appelshäuser,[35] N. Arbor,[36] S. Arcelli,[9] N. Armesto,[37] R. Arnaldi,[7] T. Aronsson,[15] I. C. Arsene,[29,38] M. Arslandok,[35] A. Augustinus,[5] R. Averbeck,[29] T. C. Awes,[39] M. D. Azmi,[12,40] M. Bach,[23] A. Badalà,[41] Y. W. Baek,[42,43] S. Bagnasco,[7] R. Bailhache,[35] V. Bairathi,[44] R. Bala,[45] A. Baldisseri,[46] F. Baltasar Dos Santos Pedrosa,[5] J. Bán,[47] R. C. Baral,[48] R. Barbera,[49] F. Barile,[24] G. G. Barnaföldi,[8] L. S. Barnby,[18] V. Barret,[43] J. Bartke,[50] M. Basile,[9] N. Bastid,[43] S. Basu,[11] B. Bathen,[31] G. Batigne,[34] B. Batyunya,[51] P. C. Batzing,[38] C. Baumann,[35] I. G. Bearden,[52] H. Beck,[35] C. Bedda,[6] N. K. Behera,[10] I. Belikov,[53] F. Bellini,[9] R. Bellwied,[54] E. Belmont-Moreno,[55] G. Bencedi,[8] S. Beole,[56] I. Berceanu,[28] A. Bercuci,[28] Y. Berdnikov,[57,58] D. Berenyi,[8] M. E. Berger,[59] A. A. E. Bergognon,[34] R. A. Bertens,[60] D. Berzano,[56] L. Betev,[5] A. Bhasin,[45] A. K. Bhati,[4] B. Bhattacharjee,[61] J. Bhom,[62] L. Bianchi,[56] N. Bianchi,[63] C. Bianchin,[60] J. Bielčík,[2] J. Bielčíková,[3] A. Bilandzic,[52] S. Bjelogrlic,[60] F. Blanco,[64] D. Blau,[17] C. Blume,[35] F. Bock,[30,65] F. V. Boehmer,[59] A. Bogdanov,[66] H. Bøggild,[52] M. Bogolyubsky,[67] L. Boldizsár,[8] M. Bombara,[68] J. Book,[35] H. Borel,[46] A. Borissov,[69,70] J. Bornschein,[23] F. Bossú,[71] M. Botje,[72] E. Botta,[56] S. Böttger,[73] P. Braun-Munzinger,[29] M. Bregant,[27,34] T. Breitner,[73] T. A. Broker,[35] T. A. Browning,[74] M. Broz,[75] E. Bruna,[7] G. E. Bruno,[24] D. Budnikov,[76]

H. Buesching,[35] S. Bufalino,[7] P. Buncic,[5] O. Busch,[30] Z. Buthelezi,[71] D. Caffarri,[77] X. Cai,[78] H. Caines,[15] A. Caliva,[60] E. Calvo Villar,[79] P. Camerini,[80] V. Canoa Roman,[5] F. Carena,[5] W. Carena,[5] F. Carminati,[5] A. Casanova Díaz,[63] J. Castillo Castellanos,[46] E. A. R. Casula,[81] V. Catanescu,[28] C. Cavicchioli,[5] C. Ceballos Sanchez,[82] J. Cepila,[2] P. Cerello,[7] B. Chang,[83] S. Chapeland,[5] J. L. Charvet,[46] S. Chattopadhyay,[11] S. Chattopadhyay,[84] M. Cherney,[85] C. Cheshkov,[86] B. Cheynis,[86] V. Chibante Barroso,[5] D. D. Chinellato,[54,87] P. Chochula,[5] M. Chojnacki,[52] S. Choudhury,[11] P. Christakoglou,[72] C. H. Christensen,[52] P. Christiansen,[88] T. Chujo,[62] S. U. Chung,[69] C. Cicalo,[89] L. Cifarelli,[9,19] F. Cindolo,[20] J. Cleymans,[40] F. Colamaria,[24] D. Colella,[24] A. Collu,[81] M. Colocci,[9] G. Conesa Balbastre,[36] Z. Conesa del Valle,[5,90] M. E. Connors,[15] G. Contin,[80] J. G. Contreras,[91] T. M. Cormier,[39,70] Y. Corrales Morales,[56] P. Cortese,[92] I. Cortés Maldonado,[93] M. R. Cosentino,[27,65] F. Costa,[5] P. Crochet,[43] R. Cruz Albino,[91] E. Cuautle,[94] L. Cunqueiro,[5,63] A. Dainese,[33] R. Dang,[78] A. Danu,[95] D. Das,[84] I. Das,[90] K. Das,[84] S. Das,[96] A. Dash,[87] S. Dash,[10] S. De,[11] H. Delagrange,[34,*] A. Deloff,[97] E. Dénes,[8] G. D'Erasmo,[24] G. O. V. de Barros,[27] A. De Caro,[19,98] G. de Cataldo,[99] J. de Cuveland,[23] A. De Falco,[81] D. De Gruttola,[19,98] N. De Marco,[7] S. De Pasquale,[98] R. de Rooij,[60] M. A. Diaz Corchero,[64] T. Dietel,[31,40] R. Divià,[5] D. Di Bari,[24] S. Di Liberto,[100] A. Di Mauro,[5] P. Di Nezza,[63] Ø. Djuvsland,[25] A. Dobrin,[60,70] T. Dobrowolski,[97] D. Domenicis Gimenez,[27] B. Dönigus,[35] O. Dordic,[38] S. Dorheim,[59] A. K. Dubey,[11] A. Dubla,[60] L. Ducroux,[86] P. Dupieux,[43] A. K. Dutta Majumdar,[84] D. Elia,[99] H. Engel,[73] B. Erazmus,[5,34] H. A. Erdal,[22] D. Eschweiler,[23] B. Espagnon,[90] M. Estienne,[34] S. Esumi,[62] D. Evans,[18] S. Evdokimov,[67] G. Eyyubova,[38] D. Fabris,[33] J. Faivre,[36] D. Falchieri,[9] A. Fantoni,[63] M. Fasel,[30] D. Fehlker,[25] L. Feldkamp,[31] D. Felea,[95] A. Feliciello,[7] G. Feofilov,[26] J. Ferencei,[3] A. Fernández Téllez,[93] E. G. Ferreiro,[37] A. Ferretti,[56] A. Festanti,[77] J. Figiel,[50] M. A. S. Figueredo,[27,101] S. Filchagin,[76] D. Finogeev,[102] F. M. Fionda,[24] E. M. Fiore,[24] E. Floratos,[103] M. Floris,[5] S. Foertsch,[71] P. Foka,[29] S. Fokin,[17] E. Fragiacomo,[104] A. Francescon,[5,77] U. Frankenfeld,[29] U. Fuchs,[5] C. Furget,[36] M. Fusco Girard,[98] J. J. Gaardhøje,[52] M. Gagliardi,[56] M. Gallio,[56] D. R. Gangadharan,[65,105] P. Ganoti,[39,103] C. Garabatos,[29] E. Garcia-Solis,[106] C. Gargiulo,[5] I. Garishvili,[1] J. Gerhard,[23] M. Germain,[34] A. Gheata,[5] M. Gheata,[5,95] B. Ghidini,[24] P. Ghosh,[11] S. K. Ghosh,[96] P. Gianotti,[63] P. Giubellino,[5] E. Gladysz-Dziadus,[50] P. Glässel,[30] R. Gomez,[91] P. González-Zamora,[64] S. Gorbunov,[23] L. Görlich,[50] S. Gotovac,[107] L. K. Graczykowski,[108] R. Grajcarek,[30] A. Grelli,[60] A. Grigoras,[5] C. Grigoras,[5] V. Grigoriev,[66] A. Grigoryan,[109] S. Grigoryan,[51] B. Grinyov,[21] N. Grion,[104] J. F. Grosse-Oetringhaus,[5] J.-Y. Grossiord,[86] R. Grosso,[5] F. Guber,[102] R. Guernane,[36] B. Guerzoni,[9] M. Guilbaud,[86] K. Gulbrandsen,[52] H. Gulkanyan,[109] T. Gunji,[110] A. Gupta,[45] R. Gupta,[45] K. H. Khan,[13] R. Haake,[31] Ø. Haaland,[25] C. Hadjidakis,[90] M. Haiduc,[95] H. Hamagaki,[110] G. Hamar,[8] L. D. Hanratty,[18] A. Hansen,[52] J. W. Harris,[15] H. Hartmann,[23] A. Harton,[106] D. Hatzifotiadou,[20] S. Hayashi,[110] A. Hayrapetyan,[5,109] S. T. Heckel,[35] M. Heide,[31] H. Helstrup,[22] A. Herghelegiu,[28] G. Herrera Corral,[91] B. A. Hess,[111] K. F. Hetland,[22] B. Hicks,[15] B. Hippolyte,[53] J. Hladky,[112] P. Hristov,[5] M. Huang,[25] T. J. Humanic,[105] D. Hutter,[23] D. S. Hwang,[113] J.-C. Ianigro,[86] R. Ilkaev,[76] I. Ilkiv,[97] M. Inaba,[62] E. Incani,[81] G. M. Innocenti,[56] C. Ionita,[5] M. Ippolitov,[17] M. Irfan,[12] M. Ivanov,[29] V. Ivanov,[57] O. Ivanytskyi,[21] A. Jachołkowski,[49] C. Jahnke,[27] H. J. Jang,[14] M. A. Janik,[108] P. H. S. Y. Jayarathna,[54] S. Jena,[10,54] R. T. Jimenez Bustamante,[94] P. G. Jones,[18] H. Jung,[42] A. Jusko,[18] S. Kalcher,[23] P. Kalinak,[47] A. Kalweit,[5] J. Kamin,[35] J. H. Kang,[114] V. Kaplin,[66] S. Kar,[11] A. Karasu Uysal,[115] O. Karavichev,[102] T. Karavicheva,[102] E. Karpechev,[102] U. Kebschull,[73] R. Keidel,[116] B. Ketzer,[59,117] M. Mohisin. Khan,[12,118] P. Khan,[84] S. A. Khan,[11] A. Khanzadeev,[57] Y. Kharlov,[67] B. Kileng,[22] B. Kim,[114] D. W. Kim,[14,42] D. J. Kim,[83] J. S. Kim,[42] M. Kim,[42] M. Kim,[114] S. Kim,[113] T. Kim,[114] S. Kirsch,[23] I. Kisel,[23] S. Kiselev,[16] A. Kisiel,[108] G. Kiss,[8] J. L. Klay,[119] J. Klein,[30] C. Klein-Bösing,[31] A. Kluge,[5] M. L. Knichel,[29] A. G. Knospe,[120] C. Kobdaj,[5,121] M. K. Köhler,[29] T. Kollegger,[23] A. Kolojvari,[26] V. Kondratiev,[26] N. Kondratyeva,[66] A. Konevskikh,[102] V. Kovalenko,[26] M. Kowalski,[50] S. Kox,[36] G. Koyithatta Meethaleveedu,[10] J. Kral,[83] I. Králik,[47] F. Kramer,[35] A. Kravčáková,[68] M. Krelina,[2] M. Kretz,[23] M. Krivda,[18,47] F. Krizek,[3,122] M. Krus,[2] E. Kryshen,[5,57] M. Krzewicki,[29] V. Kučera,[3] Y. Kucheriaev,[17] T. Kugathasan,[5] C. Kuhn,[53] P. G. Kuijer,[72] I. Kulakov,[35] J. Kumar,[10] P. Kurashvili,[97] A. Kurepin,[102] A. B. Kurepin,[102] A. Kuryakin,[76] S. Kushpil,[3] V. Kushpil,[3] M. J. Kweon,[30,123] Y. Kwon,[114] P. Ladron de Guevara,[94] C. Lagana Fernandes,[27] I. Lakomov,[90] R. Langoy,[124] C. Lara,[73] A. Lardeux,[34] A. Lattuca,[56] S. L. La Pointe,[7,60] P. La Rocca,[49] R. Lea,[80] G. R. Lee,[18] I. Legrand,[5] J. Lehnert,[35] R. C. Lemmon,[125] M. Lenhardt,[29] V. Lenti,[99] E. Leogrande,[60] M. Leoncino,[56] I. León Monzón,[126] P. Lévai,[8] S. Li,[43,78] J. Lien,[25,124] R. Lietava,[18] S. Lindal,[38] V. Lindenstruth,[23] C. Lippmann,[29] M. A. Lisa,[105] H. M. Ljunggren,[88] D. F. Lodato,[60] P. I. Loenne,[25] V. R. Loggins,[70] V. Loginov,[66] D. Lohner,[30] C. Loizides,[65] X. Lopez,[43] E. López Torres,[82] X.-G. Lu,[30] P. Luettig,[35] M. Lunardon,[77] J. Luo,[78] G. Luparello,[60] C. Luzzi,[5] A. M. Gago,[79] P. M. Jacobs,[65] R. Ma,[15] A. Maevskaya,[102] M. Mager,[5] D. P. Mahapatra,[48] A. Maire,[30,53] M. Malaev,[57] I. Maldonado Cervantes,[94] L. Malinina,[51,127] D. Mal'Kevich,[16] P. Malzacher,[29] A. Mamonov,[76] L. Manceau,[7] V. Manko,[17] F. Manso,[43] V. Manzari,[5,99] M. Marchisone,[43,56] J. Mareš,[112] G. V. Margagliotti,[80] A. Margotti,[20] A. Marín,[29] C. Markert,[5,120] M. Marquard,[35] I. Martashvili,[128] N. A. Martin,[29] P. Martinengo,[5] M. I. Martínez,[93] G. Martínez García,[34] J. Martin Blanco,[34] Y. Martynov,[21] A. Mas,[34] S. Masciocchi,[29] M. Masera,[56] A. Masoni,[89] L. Massacrier,[34] A. Mastroserio,[24] A. Matyja,[50] C. Mayer,[50] J. Mazer,[128] R. Mazumder,[129] M. A. Mazzoni,[100] F. Meddi,[130] A. Menchaca-Rocha,[55] J. Mercado Pérez,[30] M. Meres,[75] Y. Miake,[62] K. Mikhaylov,[16,51] L. Milano,[5] J. Milosevic,[38,131] A. Mischke,[60] A. N. Mishra,[129] D. Miśkowiec,[29] C. M. Mitu,[95] J. Mlynarz,[70] B. Mohanty,[11,132] L. Molnar,[53] L. Montaño Zetina,[91] E. Montes,[64] M. Morando,[77] D. A. Moreira De Godoy,[27] S. Moretto,[77] A. Morreale,[34,83] A. Morsch,[5] V. Muccifora,[63] E. Mudnic,[107] S. Muhuri,[11] M. Mukherjee,[11] H. Müller,[5] M. G. Munhoz,[27] S. Murray,[40,71] L. Musa,[5] J. Musinsky,[47] B. K. Nandi,[10] R. Nania,[20] E. Nappi,[99] C. Nattrass,[128] T. K. Nayak,[11] S. Nazarenko,[76] A. Nedosekin,[16] M. Nicassio,[29] M. Niculescu,[5,95] B. S. Nielsen,[52] S. Nikolaev,[17] S. Nikulin,[17] V. Nikulin,[57] B. S. Nilsen,[85]

F. Noferini,[19,20] P. Nomokonov,[51] G. Nooren,[60] A. Nyanin,[17] A. Nyatha,[10] J. Nystrand,[25] H. Oeschler,[30,133] S. Oh,[15] S. K. Oh,[42,134] A. Okatan,[115] L. Olah,[8] J. Oleniacz,[108] A. C. Oliveira Da Silva,[27] J. Onderwaater,[29] C. Oppedisano,[7] A. Ortiz Velasquez,[88] A. Oskarsson,[88] J. Otwinowski,[29] K. Oyama,[30] Y. Pachmayer,[30] M. Pachr,[2] P. Pagano,[98] G. Paić,[94] F. Painke,[23] C. Pajares,[37] S. K. Pal,[11] A. Palmeri,[41] D. Pant,[10] V. Papikyan,[109] G. S. Pappalardo,[41] W. J. Park,[29] A. Passfeld,[31] D. I. Patalakha,[67] V. Paticchio,[99] B. Paul,[84] T. Pawlak,[108] T. Peitzmann,[60] H. Pereira Da Costa,[46] E. Pereira De Oliveira Filho,[27] D. Peresunko,[17] C. E. Pérez Lara,[72] W. Peryt,[108,*] A. Pesci,[20] Y. Pestov,[135] V. Petráček,[2] M. Petran,[2] M. Petris,[28] M. Petrovici,[28] C. Petta,[49] S. Piano,[104] M. Pikna,[75] P. Pillot,[34] O. Pinazza,[5,20] L. Pinsky,[54] D. B. Piyarathna,[54] M. Planinic,[32,136] M. Płoskoń,[65] J. Pluta,[108] S. Pochybova,[8] P. L. M. Podesta-Lerma,[126] M. G. Poghosyan,[5,85] E. H. O. Pohjoisaho,[122] B. Polichtchouk,[67] N. Poljak,[32,136] A. Pop,[28] S. Porteboeuf-Houssais,[43] J. Porter,[65] V. Pospisil,[2] B. Potukuchi,[45] S. K. Prasad,[70,96] R. Preghenella,[19,20] F. Prino,[7] C. A. Pruneau,[70] I. Pshenichnov,[102] G. Puddu,[81] P. Pujahari,[10,70] V. Punin,[76] J. Putschke,[70] H. Qvigstad,[38] A. Rachevski,[104] S. Raha,[96] J. Rak,[83] A. Rakotozafindrabe,[46] L. Ramello,[92] R. Raniwala,[44] S. Raniwala,[44] S. S. Räsänen,[122] B. T. Rascanu,[35] D. Rathee,[4] A. W. Rauf,[13] V. Razazi,[81] K. F. Read,[128] J. S. Real,[36] K. Redlich,[97,137] R. J. Reed,[15] A. Rehman,[25] P. Reichelt,[35] M. Reicher,[60] F. Reidt,[5] R. Renfordt,[35] A. R. Reolon,[63] A. Reshetin,[102] F. Rettig,[23] J.-P. Revol,[5] K. Reygers,[30] V. Riabov,[57] R. A. Ricci,[138] T. Richert,[88] M. Richter,[38] P. Riedler,[5] W. Riegler,[5] F. Riggi,[49] A. Rivetti,[7] E. Rocco,[60] M. Rodríguez Cahuantzi,[93] A. Rodriguez Manso,[72] K. Røed,[38] E. Rogochaya,[51] S. Rohni,[45] D. Rohr,[23] D. Röhrich,[25] R. Romita,[101,125] F. Ronchetti,[63] L. Ronflette,[34] P. Rosnet,[43] S. Rossegger,[5] A. Rossi,[5] A. Roy,[129] C. Roy,[53] P. Roy,[84] A. J. Rubio Montero,[64] R. Rui,[80] R. Russo,[56] E. Ryabinkin,[17] Y. Ryabov,[57] A. Rybicki,[50] S. Sadovsky,[67] K. Šafařík,[5] B. Sahlmuller,[35] R. Sahoo,[129] P. K. Sahu,[48] J. Saini,[11] C. A. Salgado,[37] J. Salzwedel,[105] S. Sambyal,[45] V. Samsonov,[57] X. Sanchez Castro,[53,94] F. J. Sánchez Rodríguez,[126] L. Šándor,[47] A. Sandoval,[55] M. Sano,[62] G. Santagati,[49] D. Sarkar,[11] E. Scapparone,[20] F. Scarlassara,[77] R. P. Scharenberg,[74] C. Schiaua,[28] R. Schicker,[30] C. Schmidt,[29] H. R. Schmidt,[111] S. Schuchmann,[35] J. Schukraft,[5] M. Schulc,[2] T. Schuster,[15] Y. Schutz,[5,34] K. Schwarz,[29] K. Schweda,[29] G. Scioli,[9] E. Scomparin,[7] P. A. Scott,[18] R. Scott,[128] G. Segato,[77] J. E. Seger,[85] I. Selyuzhenkov,[29] J. Seo,[69] E. Serradilla,[55,64] A. Sevcenco,[95] A. Shabetai,[34] G. Shabratova,[51] R. Shahoyan,[5] A. Shangaraev,[67] N. Sharma,[48,128] S. Sharma,[45] K. Shigaki,[139] K. Shtejer,[56] Y. Sibiriak,[17] S. Siddhanta,[89] T. Siemiarczuk,[97] D. Silvermyr,[39] C. Silvestre,[36] G. Simatovic,[136] R. Singaraju,[11] R. Singh,[45] S. Singha,[11,132] V. Singhal,[11] B. C. Sinha,[11] T. Sinha,[84] B. Sitar,[75] M. Sitta,[92] T. B. Skaali,[38] K. Skjerdal,[25] R. Smakal,[2] N. Smirnov,[15] R. J. M. Snellings,[60] C. Søgaard,[88] R. Soltz,[1] J. Song,[69] M. Song,[114] F. Soramel,[77] S. Sorensen,[128] M. Spacek,[2] I. Sputowska,[50] M. Spyropoulou-Stassinaki,[103] B. K. Srivastava,[74] J. Stachel,[30] I. Stan,[95] G. Stefanek,[97] M. Steinpreis,[105] E. Stenlund,[88] G. Steyn,[71] J. H. Stiller,[30] D. Stocco,[34] M. Stolpovskiy,[67] P. Strmen,[75] A. A. P. Suaide,[27] M. A. Subieta Vasquez,[56] T. Sugitate,[139] C. Suire,[90] M. Suleymanov,[13] R. Sultanov,[16] M. Šumbera,[3] T. Susa,[32] T. J. M. Symons,[65] A. Szanto de Toledo,[27] I. Szarka,[75] A. Szczepankiewicz,[5] M. Szymanski,[108] J. Takahashi,[87] M. A. Tangaro,[24] J. D. Tapia Takaki,[90,140] A. Tarantola Peloni,[35] A. Tarazona Martinez,[5] A. Tauro,[5] G. Tejeda Muñoz,[93] A. Telesca,[5] C. Terrevoli,[24] A. Ter Minasyan,[17,66] J. Thäder,[29] D. Thomas,[60] R. Tieulent,[86] A. R. Timmins,[54] A. Toia,[33,35] H. Torii,[110] V. Trubnikov,[21] W. H. Trzaska,[83] T. Tsuji,[110] A. Tumkin,[76] R. Turrisi,[33] T. S. Tveter,[38] J. Ulery,[35] K. Ullaland,[25] J. Ulrich,[73] A. Uras,[86] G. L. Usai,[81] M. Vajzer,[3] M. Vala,[47,51] L. Valencia Palomo,[43,90] S. Vallero,[30,56] P. Vande Vyvre,[5] L. Vannucci,[138] J. W. Van Hoorne,[5] M. van Leeuwen,[60] A. Vargas,[93] R. Varma,[10] M. Vasileiou,[103] A. Vasiliev,[17] V. Vechernin,[26] M. Veldhoen,[60] M. Venaruzzo,[80] E. Vercellin,[56] S. Vergara Limón,[93] R. Vernet,[141] M. Verweij,[70] L. Vickovic,[107] G. Viesti,[77] J. Viinikainen,[83] Z. Vilakazi,[71] O. Villalobos Baillie,[18] A. Vinogradov,[17] L. Vinogradov,[26] Y. Vinogradov,[76] T. Virgili,[98] Y. P. Viyogi,[11] A. Vodopyanov,[51] M. A. Völkl,[30] K. Voloshin,[16] S. A. Voloshin,[70] G. Volpe,[5] B. von Haller,[5] I. Vorobyev,[26] D. Vranic,[5,29] J. Vrláková,[68] B. Vulpescu,[43] A. Vyushin,[76] B. Wagner,[25] J. Wagner,[29] V. Wagner,[2] M. Wang,[34,78] Y. Wang,[30] D. Watanabe,[62] M. Weber,[54] J. P. Wessels,[31] U. Westerhoff,[31] J. Wiechula,[111] J. Wikne,[38] M. Wilde,[31] G. Wilk,[97] J. Wilkinson,[30] M. C. S. Williams,[20] B. Windelband,[30] M. Winn,[30] C. Xiang,[78] C. G. Yaldo,[70] Y. Yamaguchi,[110] H. Yang,[46,60] P. Yang,[78] S. Yang,[25] S. Yano,[139] S. Yasnopolskiy,[17] J. Yi,[69] Z. Yin,[78] I.-K. Yoo,[69] I. Yushmanov,[17] V. Zaccolo,[52] C. Zach,[2] A. Zaman,[13] C. Zampolli,[20] S. Zaporozhets,[51] A. Zarochentsev,[26] P. Závada,[112] N. Zaviyalov,[76] H. Zbroszczyk,[108] I. S. Zgura,[95] M. Zhalov,[57] F. Zhang,[78] H. Zhang,[78] X. Zhang,[43,65,78] Y. Zhang,[78] C. Zhao,[38] D. Zhou,[78] F. Zhou,[78] Y. Zhou,[60] H. Zhu,[78] J. Zhu,[78] J. Zhu,[78] X. Zhu,[78] A. Zichichi,[9,19] A. Zimmermann,[30] M. B. Zimmermann,[5,31] G. Zinovjev,[21] Y. Zoccarato,[86] M. Zynovyev,[21] and M. Zyzak[35]

(ALICE Collaboration)

[1]*Lawrence Livermore National Laboratory, Livermore, California 94550, USA*
[2]*Faculty of Nuclear Sciences and Physical Engineering, Czech Technical University in Prague, Prague, Czech Republic*
[3]*Nuclear Physics Institute, Academy of Sciences of the Czech Republic, Řež u Prahy, Czech Republic*
[4]*Physics Department, Panjab University, Chandigarh, India*
[5]*European Organization for Nuclear Research (CERN), Geneva, Switzerland*
[6]*Politecnico di Torino, Turin, Italy*
[7]*Sezione INFN, Turin, Italy*
[8]*Wigner Research Centre for Physics, Hungarian Academy of Sciences, Budapest, Hungary*
[9]*Dipartimento di Fisica e Astronomia dell'Università and Sezione INFN, Bologna, Italy*

[10]*Indian Institute of Technology Bombay (IIT), Mumbai, India*
[11]*Variable Energy Cyclotron Centre, Kolkata, India*
[12]*Department of Physics, Aligarh Muslim University, Aligarh, India*
[13]*COMSATS Institute of Information Technology (CIIT), Islamabad, Pakistan*
[14]*Korea Institute of Science and Technology Information, Daejeon, South Korea*
[15]*Yale University, New Haven, Connecticut 06520, USA*
[16]*Institute for Theoretical and Experimental Physics, Moscow, Russia*
[17]*Russian Research Centre Kurchatov Institute, Moscow, Russia*
[18]*School of Physics and Astronomy, University of Birmingham, Birmingham, United Kingdom*
[19]*Centro Fermi-Museo Storico della Fisica e Centro Studi e Ricerche "Enrico Fermi," Rome, Italy*
[20]*Sezione INFN, Bologna, Italy*
[21]*Bogolyubov Institute for Theoretical Physics, Kiev, Ukraine*
[22]*Faculty of Engineering, Bergen University College, Bergen, Norway*
[23]*Frankfurt Institute for Advanced Studies, Johann Wolfgang Goethe-Universität Frankfurt, Frankfurt, Germany*
[24]*Dipartimento Interateneo di Fisica "M. Merlin" and Sezione INFN, Bari, Italy*
[25]*Department of Physics and Technology, University of Bergen, Bergen, Norway*
[26]*V. Fock Institute for Physics, Saint Petersburg State University, St. Petersburg, Russia*
[27]*Universidade de São Paulo (USP), São Paulo, Brazil*
[28]*National Institute for Physics and Nuclear Engineering, Bucharest, Romania*
[29]*Research Division and ExtreMe Matter Institute EMMI, GSI Helmholtzzentrum für Schwerionenforschung, Darmstadt, Germany*
[30]*Physikalisches Institut, Ruprecht-Karls-Universität Heidelberg, Heidelberg, Germany*
[31]*Institut für Kernphysik, Westfälische Wilhelms-Universität Münster, Münster, Germany*
[32]*Rudjer Bošković Institute, Zagreb, Croatia*
[33]*Sezione INFN, Padova, Italy*
[34]*SUBATECH, Ecole des Mines de Nantes, Université de Nantes, CNRS-IN2P3, Nantes, France*
[35]*Institut für Kernphysik, Johann Wolfgang Goethe-Universität Frankfurt, Frankfurt, Germany*
[36]*Laboratoire de Physique Subatomique et de Cosmologie (LPSC), Université Joseph Fourier, CNRS-IN2P3, Institut Polytechnique de Grenoble, Grenoble, France*
[37]*Departamento de Física de Partículas and IGFAE, Universidad de Santiago de Compostela, Santiago de Compostela, Spain*
[38]*Department of Physics, University of Oslo, Oslo, Norway*
[39]*Oak Ridge National Laboratory, Oak Ridge, Tennessee 37830, USA*
[40]*Physics Department, University of Cape Town, Cape Town, South Africa*
[41]*Sezione INFN, Catania, Italy*
[42]*Gangneung-Wonju National University, Gangneung, South Korea*
[43]*Laboratoire de Physique Corpusculaire (LPC), Clermont Université, Université Blaise Pascal, CNRS-IN2P3, Clermont-Ferrand, France*
[44]*Physics Department, University of Rajasthan, Jaipur, India*
[45]*Physics Department, University of Jammu, Jammu, India*
[46]*Commissariat à l'Energie Atomique, IRFU, Saclay, France*
[47]*Institute of Experimental Physics, Slovak Academy of Sciences, Košice, Slovakia*
[48]*Institute of Physics, Bhubaneswar, India*
[49]*Dipartimento di Fisica e Astronomia dell'Università and Sezione INFN, Catania, Italy*
[50]*The Henryk Niewodniczanski Institute of Nuclear Physics, Polish Academy of Sciences, Cracow, Poland*
[51]*Joint Institute for Nuclear Research (JINR), Dubna, Russia*
[52]*Niels Bohr Institute, University of Copenhagen, Copenhagen, Denmark*
[53]*Institut Pluridisciplinaire Hubert Curien (IPHC), Université de Strasbourg, CNRS-IN2P3, Strasbourg, France*
[54]*University of Houston, Houston, Texas 77004, USA*
[55]*Instituto de Física, Universidad Nacional Autónoma de México, Mexico City, Mexico*
[56]*Dipartimento di Fisica dell'Università and Sezione INFN, Turin, Italy*
[57]*Petersburg Nuclear Physics Institute, Gatchina, Russia*
[58]*Saint Petersburg State Polytechnical University, St. Petersburg, Russia*
[59]*Technische Universität München, Munich, Germany*
[60]*Institute for Subatomic Physics of Utrecht University, Utrecht, Netherlands*
[61]*Gauhati University, Department of Physics, Guwahati, India*
[62]*University of Tsukuba, Tsukuba, Japan*
[63]*Laboratori Nazionali di Frascati, INFN, Frascati, Italy*
[64]*Centro de Investigaciones Energéticas Medioambientales y Tecnológicas (CIEMAT), Madrid, Spain*
[65]*Lawrence Berkeley National Laboratory, Berkeley, California 94704, USA*

[66]*Moscow Engineering Physics Institute, Moscow, Russia*
[67]*Institute for High Energy Physics, Protvino, Russia*
[68]*Faculty of Science, P. J. Šafárik University, Košice, Slovakia*
[69]*Pusan National University, Pusan, South Korea*
[70]*Wayne State University, Detroit, Michigan 48202, USA*
[71]*iThemba LABS, National Research Foundation, Somerset West, South Africa*
[72]*Nikhef, National Institute for Subatomic Physics, Amsterdam, Netherlands*
[73]*Institut für Informatik, Johann Wolfgang Goethe-Universität Frankfurt, Frankfurt, Germany*
[74]*Purdue University, West Lafayette, Indiana 47907, USA*
[75]*Faculty of Mathematics, Physics and Informatics, Comenius University, Bratislava, Slovakia*
[76]*Russian Federal Nuclear Center (VNIIEF), Sarov, Russia*
[77]*Dipartimento di Fisica e Astronomia dell'Università and Sezione INFN, Padova, Italy*
[78]*Central China Normal University, Wuhan, China*
[79]*Sección Física, Departamento de Ciencias, Pontificia Universidad Católica del Perú, Lima, Peru*
[80]*Dipartimento di Fisica dell'Università and Sezione INFN, Trieste, Italy*
[81]*Dipartimento di Fisica dell'Università and Sezione INFN, Cagliari, Italy*
[82]*Centro de Aplicaciones Tecnológicas y Desarrollo Nuclear (CEADEN), Havana, Cuba*
[83]*University of Jyväskylä, Jyväskylä, Finland*
[84]*Saha Institute of Nuclear Physics, Kolkata, India*
[85]*Physics Department, Creighton University, Omaha, Nebraska 68102, USA*
[86]*Université de Lyon, Université Lyon 1, CNRS/IN2P3, IPN-Lyon, Villeurbanne, France*
[87]*Universidade Estadual de Campinas (UNICAMP), Campinas, Brazil*
[88]*Division of Experimental High Energy Physics, University of Lund, Lund, Sweden*
[89]*Sezione INFN, Cagliari, Italy*
[90]*Institut de Physique Nucleaire d'Orsay (IPNO), Universite Paris-Sud, CNRS-IN2P3, Orsay, France*
[91]*Centro de Investigación y de Estudios Avanzados (CINVESTAV), Mexico City and Mérida, Mexico*
[92]*Dipartimento di Scienze e Innovazione Tecnologica dell'Università del Piemonte Orientale and Gruppo Collegato INFN, Alessandria, Italy*
[93]*Benemérita Universidad Autónoma de Puebla, Puebla, Mexico*
[94]*Instituto de Ciencias Nucleares, Universidad Nacional Autónoma de México, Mexico City, Mexico*
[95]*Institute of Space Science (ISS), Bucharest, Romania*
[96]*Bose Institute, Department of Physics and Centre for Astroparticle Physics and Space Science (CAPSS), Kolkata, India*
[97]*National Centre for Nuclear Studies, Warsaw, Poland*
[98]*Dipartimento di Fisica "E.R. Caianiello" dell'Università and Gruppo Collegato INFN, Salerno, Italy*
[99]*Sezione INFN, Bari, Italy*
[100]*Sezione INFN, Rome, Italy*
[101]*University of Liverpool, Liverpool, United Kingdom*
[102]*Institute for Nuclear Research, Academy of Sciences, Moscow, Russia*
[103]*Physics Department, University of Athens, Athens, Greece*
[104]*Sezione INFN, Trieste, Italy*
[105]*Department of Physics, Ohio State University, Columbus, Ohio 43210, USA*
[106]*Chicago State University, Chicago, Illinois 60628, USA*
[107]*Technical University of Split FESB, Split, Croatia*
[108]*Warsaw University of Technology, Warsaw, Poland*
[109]*A. I. Alikhanyan National Science Laboratory (Yerevan Physics Institute) Foundation, Yerevan, Armenia*
[110]*University of Tokyo, Tokyo, Japan*
[111]*Eberhard Karls Universität Tübingen, Tübingen, Germany*
[112]*Institute of Physics, Academy of Sciences of the Czech Republic, Prague, Czech Republic*
[113]*Department of Physics, Sejong University, Seoul, South Korea*
[114]*Yonsei University, Seoul, South Korea*
[115]*KTO Karatay University, Konya, Turkey*
[116]*Zentrum für Technologietransfer und Telekommunikation (ZTT), Fachhochschule Worms, Worms, Germany*
[117]*Excellence Cluster Universe, Technische Universität München, Munich, Germany*
[118]*Department of Applied Physics, Aligarh Muslim University, Aligarh, India*
[119]*California Polytechnic State University, San Luis Obispo, California 93407, USA*
[120]*The University of Texas at Austin, Physics Department, Austin, Texas 78712, USA*
[121]*Suranaree University of Technology, Nakhon Ratchasima, Thailand*
[122]*Helsinki Institute of Physics (HIP), Helsinki, Finland*
[123]*Inha University, College of Natural Sciences*

[124]*Vestfold University College, Tonsberg, Norway*
[125]*Nuclear Physics Group, STFC Daresbury Laboratory, Daresbury, United Kingdom*
[126]*Universidad Autónoma de Sinaloa, Culiacán, Mexico*
[127]*M. V. Lomonosov Moscow State University, D. V. Skobeltsyn Institute of Nuclear Physics, Moscow, Russia*
[128]*University of Tennessee, Knoxville, Tennessee 37996, USA*
[129]*Indian Institute of Technology Indore, Indore (IITI), India*
[130]*Dipartimento di Fisica dell'Università "La Sapienza" and Sezione INFN Rome*
[131]*University of Belgrade, Faculty of Physics and "Vinča" Institute of Nuclear Sciences, Belgrade, Serbia*
[132]*National Institute of Science Education and Research, Bhubaneswar, India*
[133]*Institut für Kernphysik, Technische Universität Darmstadt, Darmstadt, Germany*
[134]*Konkuk University, Seoul, South Korea*
[135]*Budker Institute for Nuclear Physics, Novosibirsk, Russia*
[136]*University of Zagreb, Zagreb, Croatia*
[137]*Institute of Theoretical Physics, University of Wroclaw, Wroclaw, Poland*
[138]*Laboratori Nazionali di Legnaro, INFN, Legnaro, Italy*
[139]*Hiroshima University, Hiroshima, Japan*
[140]*The University of Kansas, Lawrence, Kansas 66045, USA*
[141]*Centre de Calcul de l'IN2P3, Villeurbanne, France*

[*]Deceased.